9/26

LBL-11302
UC-11 c.2

TWO WELL STORAGE SYSTEMS FOR COMBINED HEATING AND AIRCONDITIONING BY GROUNDWATER HEATPUMPS IN SHALLOW AQUIFERS

Walter Pelka

July 1980

Prepared for the U.S. Department of Energy
under Contract W-7405-ENG-48

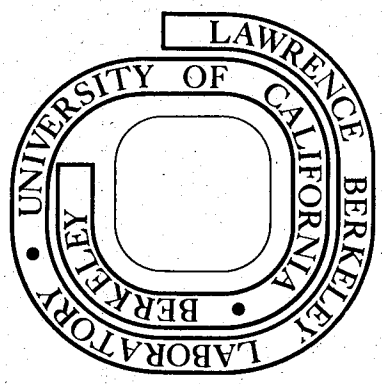

LBL-11302

TWO WELL STORAGE SYSTEMS FOR COMBINED HEATING AND AIRCONDITIONING BY GROUNDWATER HEATPUMPS IN SHALLOW AQUIFERS

By

Walter Pelka

Earth Sciences Division
Lawrence Berkeley Laboratory
University of California
Berkeley, California, USA

and

Institut fuer Wasserbau und Wasserwirtschaft
Rheinisch Westfaelische Technische Hochschule
Aachen, West Germany

LIST OF FIGURES

Figure 1.	Heating and cooling demand compared with air temperature and solar radiation (qualitative).	2
Figure 2.	Seasonal temperature distribution in an aquifer as a function of depth.	4
Figure 3.	Temperature changes of the aquifer at different depth below the surface.	4
Figure 4.	The heat pump process.	5
Figure 5.	Direct use of groundwater as a heat source.	7
Figure 6.	Indirect use of groundwater as a heat source.	8
Figure 7.	Basic two well storage system.	10
Figure 8.	Extended two well storage system.	11
Figure 9.	Iteration of the free surface by node shifting.	24
Figure 10.	Deformation of heat transport mesh and flow mesh during the iterative calculation of the free surface.	25
Figure 11.	Flow chart of iterative calculations.	27
Figure 12.	Temperature distribution over one year (daily averages).	29
Figure 13.	Vertical cross-section of the aquifer.	30
Figure 14.	Meshes for flow and heat transport calculation.	33
Figure 15a.	Flow boundary conditions.	35
Figure 15b.	Heat transport boundary conditions.	35
Figure 16.	Calculated seasonal temperature distributions in the aquifer as function of depth below the surface.	36
Figure 17.	Calculated seasonal changes of soil and groundwater temperatures in different depth below the surface	37
Figure 18.	Heating and cooling demand for 750 families.	39
Figure 19.	Cold water well injection - Boundary conditions.	41
Figure 20.	Cold water well extraction - Boundary conditions.	41

TABLE OF CONTENTS

Table of Contents	i
List of Figures	ii
List of Tables	iv
1. Introduction	1
2. Soil and Groundwater as an Energy Source	3
2.1. Natural Groundwater Temperatures	3
2.2. The Operation of a Heat Pump	5
2.3. Groundwater Heat Pump Applications	7
2.4. Two Well Storage Systems	8
2.5. Risks to the Environment	12
3. Governing Equations	14
3.1. Saturated Zone	14
3.2. Unsaturated Zone	16
4. Method of Solution	18
4.1. Analytical Solutions	18
4.2. Finite Element Approach	18
5. Examples of Two Well Storage Systems	29
5.1. Meteorological Data	29
5.2. Aquifer Data	30
5.3. Numerical Calculations	32
5.4. Natural Soil Temperature Distribution	34
5.5. Cold Water Storage	38
5.6. Cold and Warm Water Storage	52
6. Conclusions	68
List of Symbols	70
Acknowledgements	72
References	73

Figure 21. Calculated and estimated mass flow (first cycle). 43

Figure 22. Estimated and calculated recovery factor. 44

Figure 23. Available extraction temperatures. 45

Figure 24. Average temperature of the aquifer versus radius. 47

Figure 25a. Temperature distribution in vertical cross-sections (November 1). 48

Figure 25b. Temperature distribution in vertical cross-sections (February 1). 49

Figure 25c. Temperature distribution in vertical cross-sections (May 15). 50

Figure 25d. Temperature distribution in vertical cross-sections (July 15). 51

Figure 26. Extraction and injection temperatures at the cold water well and warm water well. 54

Figure 27. Heat fluxes for extraction periods. 55

Figure 28. Cumulative curve of additionally injected and extracted cooling capacity at the cold water well. 56

Figure 29. Cumulative curve of additionally injected and extracted energy at the warm water well. 57

Figure 30. Cumulative curves of total extracted energy at the warm water well. 59

Figure 31a. Temperature as function of radius (first year). 61

Figure 31b. Temperature as function of radius (second year). 62

Figure 31c. Temperature as function of radius (third year). 63

Figure 32a. Temperature distribution in vertical cross-sections (November 1). 64

Figure 32b. Temperature distribution in vertical cross-sections (February 1). 65

Figure 32c. Temperature distribution in vertical cross-sections (May 15). 66

Figure 32d. Temperature distribution in vertical cross-sections (July 15). 67

LIST OF TABLES

Table 1.	Fluid properties	31
Table 2.	Solid matrix properties of aquifer	31
Table 3.	Bedrock properties	32
Table 4.	Size of an average apartment	40
Table 5.	Total and additionally injected and extracted energy	60

1. INTRODUCTION

For highly industrialized nations the reliability of their energy supply is a matter of vital interest. Limited primary energy resources and uncertain supply form energy exporting countries are in contrast to increasing energy demands. The only practical solution to this problem is conserving energy and developing alternative energy sources. A major part of the total energy consumption goes to space heating or space cooling in offices and domestic households.

In warmer climates air source heat pumps have gained widest acceptance for air conditioning due to their commercial availability, reliability, and moderate capital costs. However, the application of air heatpumps in colder climates has several disadvantages. Obviously the air temperature is extremely low in times of great heating demand, but very high when space cooling is necessary. This together with the low heat capacity of air implies large air throughput and leads to a lack of efficiency.

The same is true for the direct use of solar energy, especially in northern climates, since during the heating season the solar radiation is at its minimum. Figure 1 shows qualitatively the heating and cooling demand compared with the air temperature and the daily available energy from solar radiation in northern climates.

Water source heat pumps have several advantages over air source heat pumps. For example, the performance coefficient is

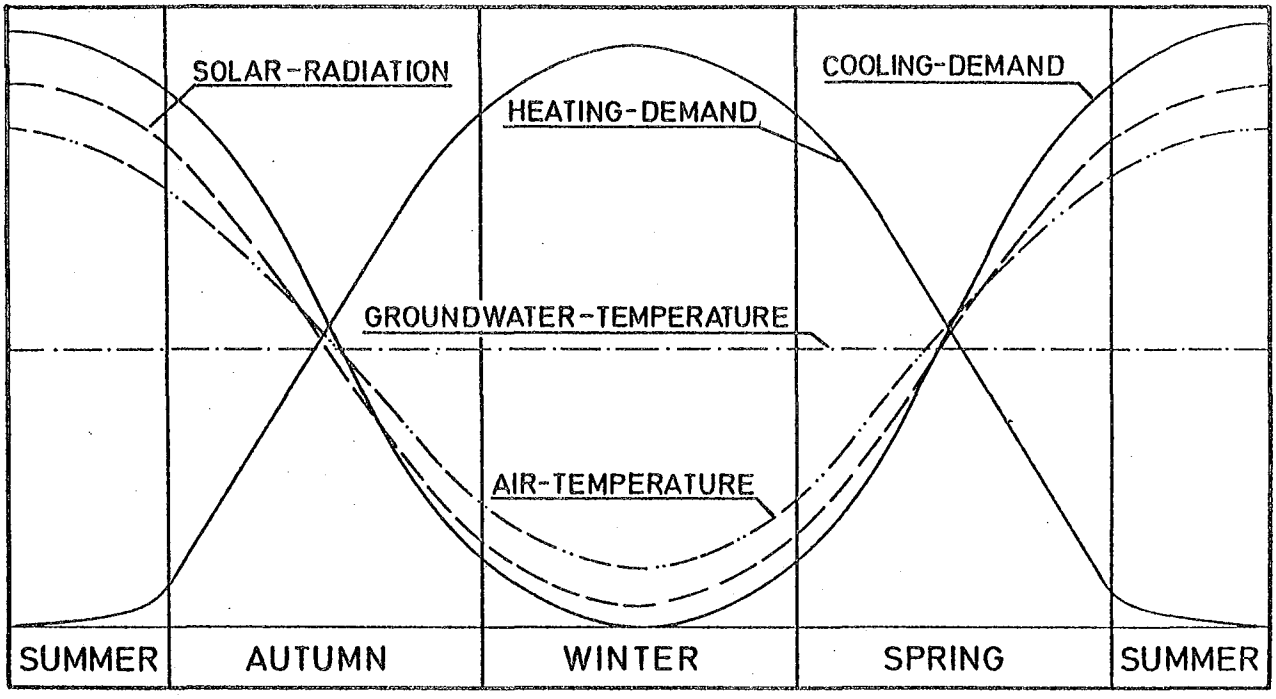

XBL 808-11151

Figure 1. Heating and cooling demand compared with air temperature and solar radiation (qualitative).

about four for today's commercially available water source equipment; whereas that for air source equipment is much less. The source for this kind of heat pump can be surface or groundwater.

2. SOIL AND GROUNDWATER AS ENERGY SOURCE

2.1 Natural Groundwater Temperatures

Temperature profiles in a vertical profile of a shallow aquifer are shown in Figure 2 for different seasons of the year (2). The seasonal changes of temperature due to changing surface temperatures decrease with increasing distance from the surface. Below a certain depth only small variations around the average temperature are detectable (Figure 3), and due to a transit time effect these oscillations may be in phase opposition to the changes in surface temperature. Because of the positive radiation balance the yearly average temperature of the groundwater is slightly higher than the average air temperature.

The energy stored in aquifers comes mainly from solar radiation with minor contributions from the internal heat of the earth. The heat from the solar radiation is transferred to the groundwater by direct recharge of solar heated surface water and conduction from the warmer surface to the aquifer, where the ground surface is heated both by radiation and surface heat transfer from the warmer air. Due to the geothermal temperature gradient heat is also transferred from the interior of the earth to the surface.

Groundwater from shallow confined or unconfined aquifers is so widely available as to make groundwater source heat pumps a realistic alternative to fossil fuel energy sources for conventional space or hot water heating in private homes and commercial buildings.

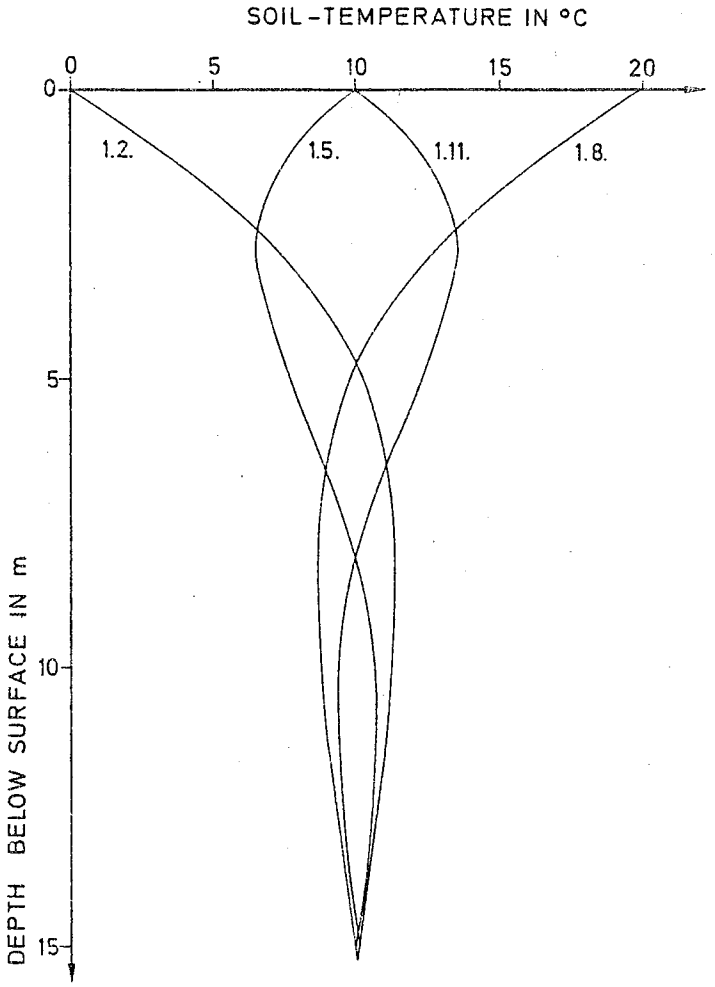

Figure 2. Seasonal temperature distribution in an aquifer as a function of depth. *XBL 808-11152*

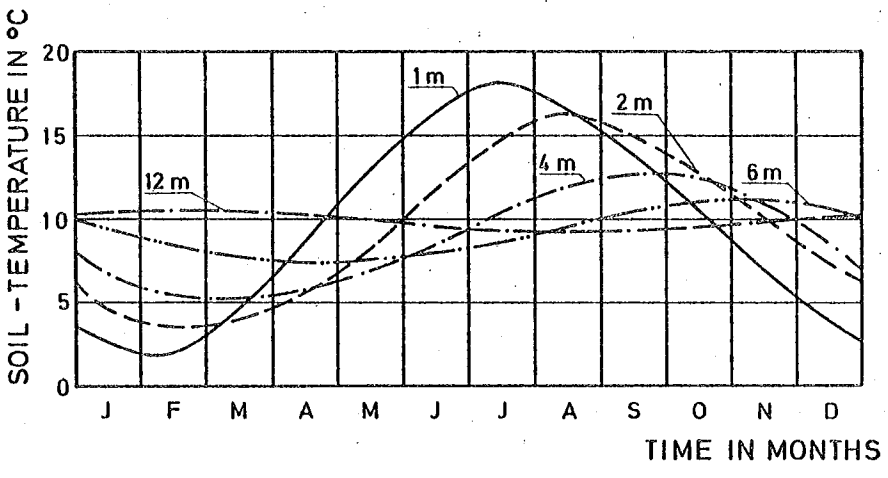

Figure 3. Temperature changes of the aquifer at different depths below the surface. *XBL 808-11153*

2.2. The Operation of a Heatpump

To understand the two well storage system and fully exploit its potential, it is important to discuss the basic physical principles of a heat pump. Figure 4 shows a schematic representation of the operation of a heat pump.

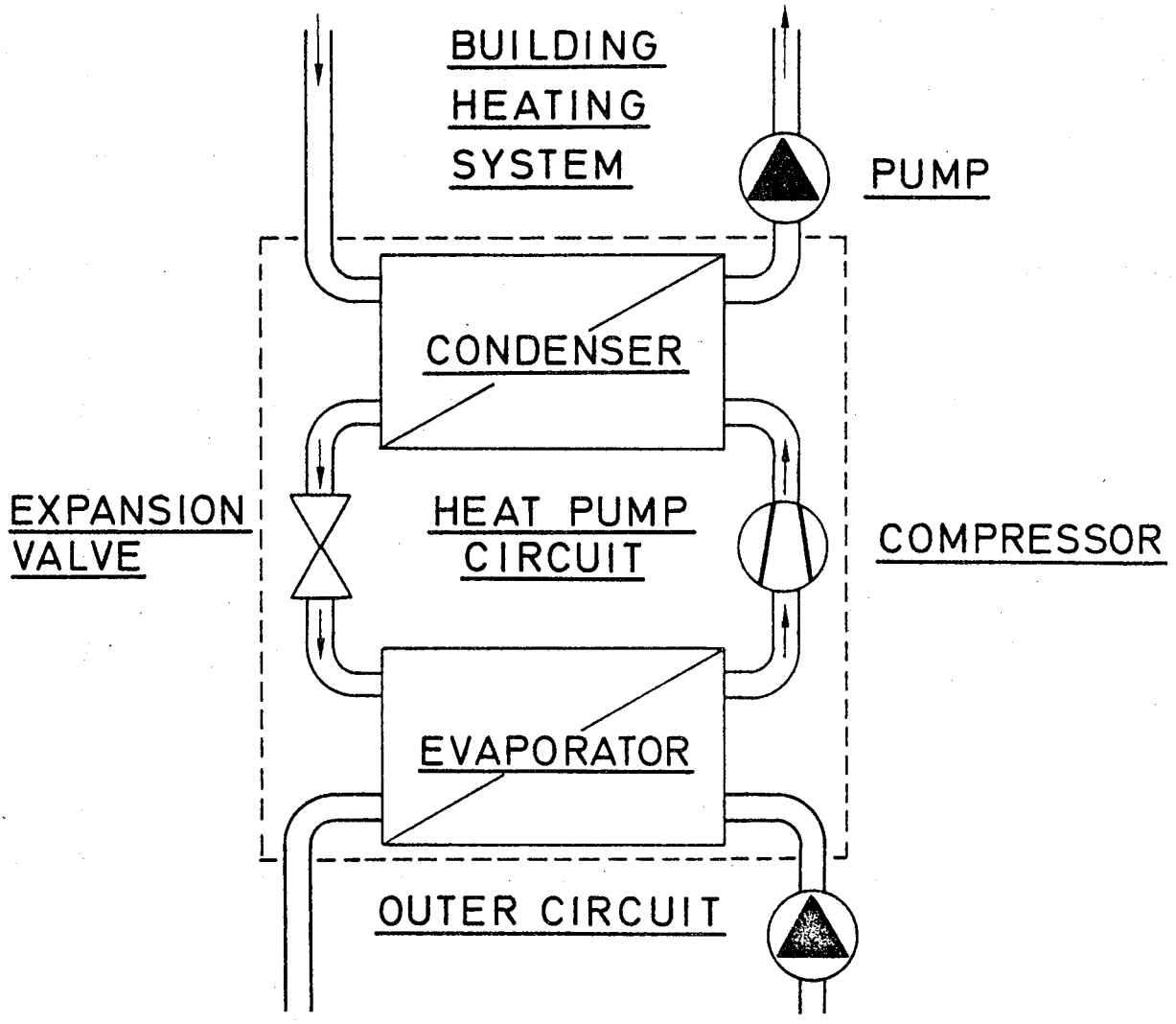

XBL 808-11154

Figure 4. The heat pump process.

In the first heat exchanger (evaporator) heat from the heat source (groundwater in this case) is transferred to the cooling fluid of the internal circuit of the heat pump. As the cooling fluid is heated, it evaporates. It is then compressed and fed into a second heat exchanger (condenser) where the heat is transferred to a building heating system.

The condensed cooling fluid is passed back to the evaporator through an expansion valve which separates the high and low pressure portion of the heat pump circuit.

The ratio between the energy moved from the heat source to another level and the energy used during this work is the coefficient of performance (COP). The COP can be calculated by,

$$COP = \left(1 + \frac{T_u}{T_i - T_u + \Delta t_c + \Delta t_e} \cdot \eta\right)$$

where

T_u	Temperature of the heat source
T_i	Temperature of the forward flow of the heating
ΔT_c	Temperature difference in the condensor
ΔT_e	Temperature difference in the evaporator
η	Efficiency coefficient

As can be seen in the above formula the COP decreases with an increase in the difference between the heat source and heating temperature. As will be seen later this must be considered in the design and operation of a two well storage system.

2.3 Groundwater Heat Pump Applications

Today two basic methods exist for using the heat stored in an aquifer by heat pumps (11). The direct method is to pump water from a well to the heat exchanger of the heat pump's outer circuit, where it is cooled several degrees and then reinjected into the aquifer by a recharge well (Figure 5).

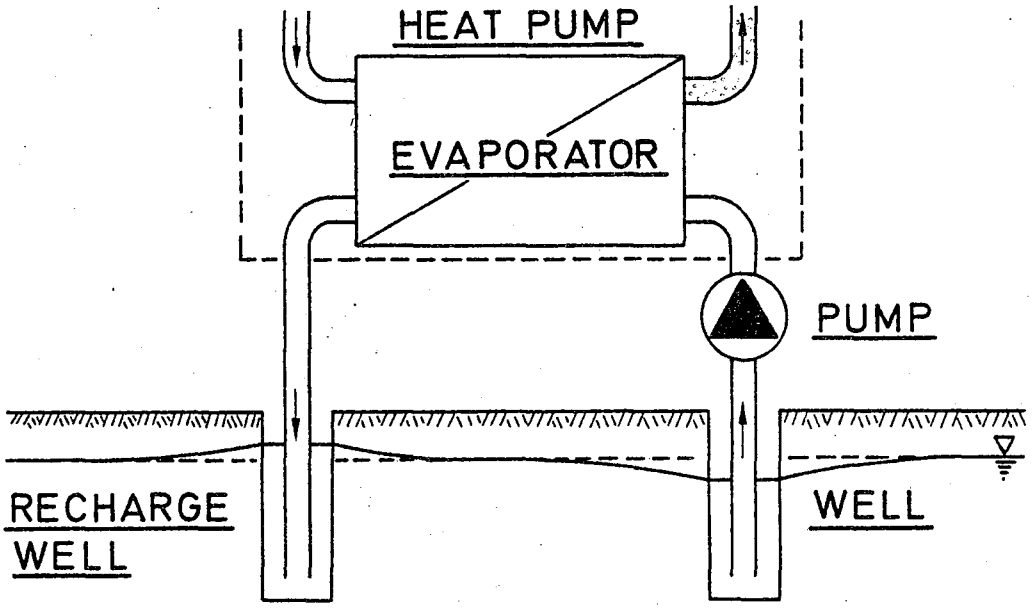

Figure 5. Direct use of groundwater as a heat source.

In the indirect method (Figure 6) a pipe system is buried in the aquifer. It may be placed either in the unsaturated, or in the saturated zone, where heat transfer to the pipe will be more efficient.

A coolant flows through these pipes and extracts heat from the surrounding earth and groundwater. The cooling fluid trans-

ports the absorbed heat to the outer heat exchanger. No groundwater is pumped to the surface and reinjected into the aquifer in this case. This method requires relatively large areas for satisfactory results in colder climates.

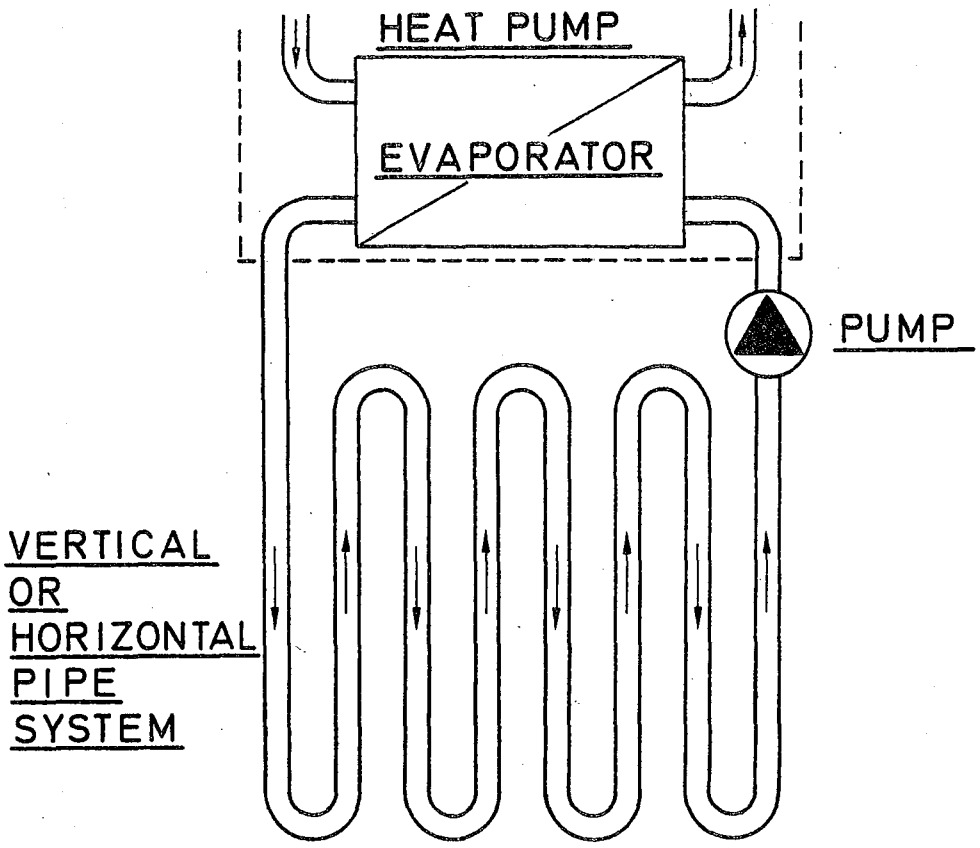

XBL 808-11156

Figure 6. Indirect use of groundwater as a heat source.

2.4 Two Well Storage Systems

In many cases, especially in more populated areas, it will not be sufficient to pump groundwater from a single well, extract

the heat and discard the cooled water into a surface water body. This could lead to depletion of the aquifer, excessive drawdown and such problems as compaction and subsidence. In order to avoid this and maintain the overall equilibrium of the aquifer, the water should be reinjected by a recharge well after use; that is, two wells should be drilled for a heat pump system.

Because of its basic construction, a heat pump can easily be used not only for space heating, but also for space cooling. Of course, this is also true for groundwater source heat pumps. A heat pump can be used to extract energy from the groundwater for space heating in winter, and also to transfer heat from an air conditioning system to the groundwater in summer.

Figure 7 illustrates the basic ideas of a two well storage system consisting of a cold water well and a warm water well. In winter, when space heating is required, water is pumped from the warm water well. The heat is extracted from the warm water by the heat pump after which the cooled water is reinjected into the aquifer using the cold water well as a recharge well. The energy extracted from the groundwater is used for heating purposes.

In summer, when space cooling might be necessary, colder water which was injected during winter is extracted from the cold water well. This water is at a temperature below the average aquifer temperature. After heat is removed from the air conditioning system by the groundwater it is injected into the warm water well at a temperature that is at or even higher than the average aquifer temperature.

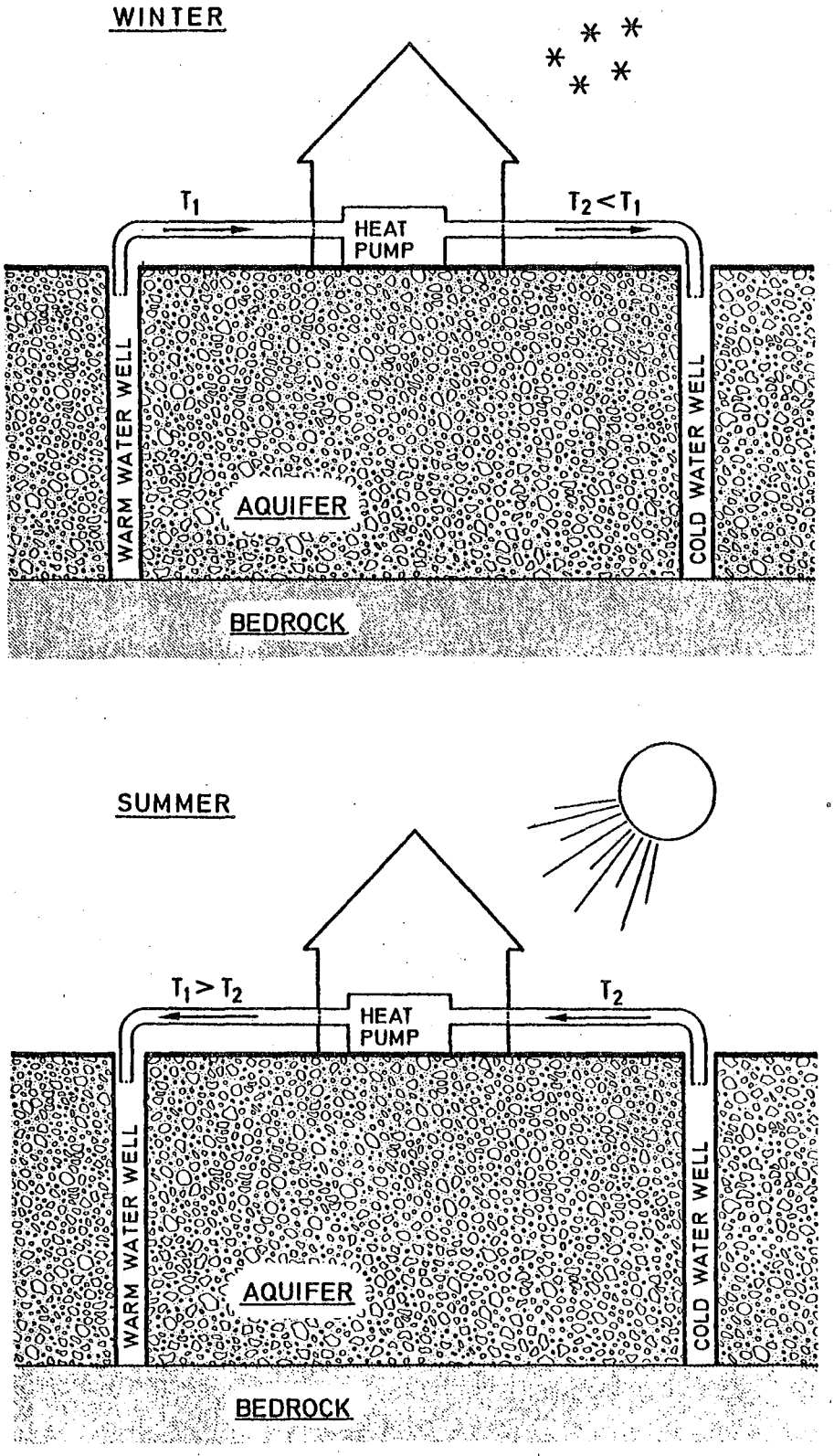

XBL 808-11157

Figure 7. Basic two well storage system.

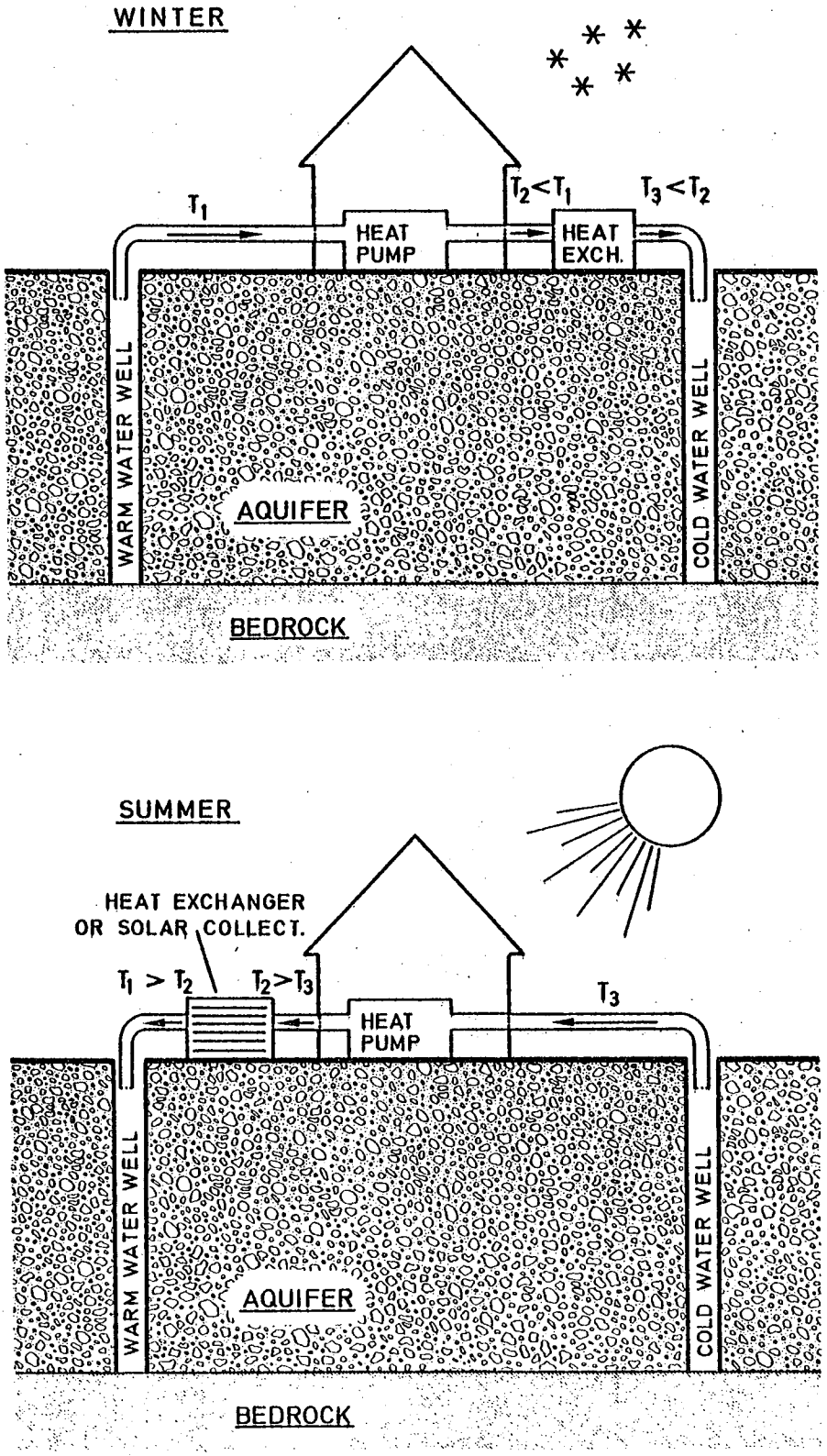

Figure 8. Extended two well storage system. *XBL 808-11158*

The efficiency of the above storage system could be improved by the further cooling of the groundwater injected in the winter or conversely heated in the summer. The problem with this approach is that using heat pumps to create large temperature differences leads to small coefficients of performance for the heat exchanger system.

One solution to this problem, shown in Figure 8, is the addition of a secondary heat exchanger. This heat exchanger is installed between the heat pump and the injection well and is exposed to the environment. In the winter the injected water is cooled another few degrees by the cold winter air. In summer the injected water is heated by the convection of warm air over the heat exchanger and solar radiation.

2.5 Risks for the Environment

Any use of an aquifer for space heating or air conditioning implies changes in the thermal field of the aquifer. This could lead to problems which should be considered before the exploitation. Extensive use of groundwater geothermal energy may be of minor importance. Nonetheless, increasing exploitation of this energy resource could lead to severe environmental damages and economical disadvantages. For example, the rise and fall of groundwater temperatures affects the biological environment and chemical equilibrium in the aquifer. In order to avoid or mimimize negative effects on the environment and to optimize the economical benefit, it is necessary to know how the thermal anomaly will

spread in the aquifer; i.e., the size of the affected area and influences on surrounding heat pumps. The efficiency to be expected should also be calculated. These issues are discussed further below.

Other risks, such as the contamination of the groundwater due to a leakage in the heat exchanger of the heat pump system, are beyond the scope of this paper.

3. GOVERNING EQUATIONS

3.1 Saturated Zone

Heat transport in flowing groundwater takes place by conduction and convection. Balancing the heat flux into and out of a small element leads to the differential equation describing the temperature distribution in an aquifer,

$$\frac{\partial T}{\partial t}\left(\rho_B C_B\right) + \frac{\partial}{\partial x_i}\left(\rho_F C_F T v_i\right) - \frac{\partial}{\partial x_i}\left(D_{ij}' \frac{\partial T}{\partial x_j}\right) = 0 \quad , \tag{1}$$

where the subscripts i and j are used for the Einstein summation convention. All other terms are defined in the list of symbols. The first term

$$\frac{\partial T}{\partial t}\left(\rho_B C_B\right) \tag{2}$$

describes the heat stored in the balance volume due to the temperature changes with time. The second term of the differential equation

$$\frac{\partial}{\partial x_i}\left(\rho_F C_F T v_i\right) \tag{3}$$

characterizes the heat transport by convection, and the third term

$$\frac{\partial}{\partial x_i}\left(D_{ij}' \frac{\partial T}{\partial x_j}\right) \tag{4}$$

represents the diffusive portion of the transport. Bulk density and bulk heat capacity ρ_B and c_B, are calculated for the saturated zone thus

$$\rho_B = \theta\rho_F + (1-\theta)\ \rho_M \tag{5}$$

and

$$C_B = \theta C_F + (1-\theta)\ C_M \tag{6}$$

The tensor of effective dispersion D_{ij}' combines mechanical dispersion and the effective heat conduction. The mechanical dispersion is a linear function of the fluid velocity (3) with longitudinal and transversal components

$$D_{ij} = a_{II}\ \delta_{ij}\ |V| + (a_I - a_{II}) \cdot \frac{V_i V_j}{|V|} \tag{7}$$

Heat conduction and mechanical dispersion are summed. The result is the tensor of effective dispersion

$$D_{ij}' = \theta\rho_F C_F D_{ij} + \Lambda_{B_{ij}} \tag{8}$$

The equation governing three-dimensional water movement in a saturated porous medium can be derived from a mass balance

$$\frac{\partial p}{\partial t}\ (\rho_F S) + \frac{\partial}{\partial x_i}\ (\rho_F q_i) = 0 \tag{9}$$

and the generalized Darcy equation

$$q_i = - \frac{k_{ij}}{\mu} \left(\frac{\partial p}{\partial x_i} - \rho_F g \frac{\partial z}{\partial x_j} \right) \tag{10}$$

By substituting equation (10) into equation (9), one obtains the basic flow equation

$$\frac{\partial p}{\partial t} (\rho_F S') - \frac{\partial}{\partial x_i} \left[\frac{\rho_F k_{ij}}{\mu} \left(\frac{\partial p}{\partial x_j} - \rho_F g \frac{\partial z}{\partial x_j} \right) \right] = 0 \quad . \tag{11}$$

Knowing the effective porosity of the porous medium, the average fluid velocity v_i can be calculated from the mass flux q_i

$$v_i = q_i / \varepsilon \tag{12}$$

The problem under consideration turns out to be a highly nonlinear one, since the dynamic viscosity and the density of the fluid in equation (11) become functions of the temperature distribution in the aquifer described by equation (1). On the other hand, the actual temperature field depends, by means of the convective term, on the velocity distribution calculated in equation (11) and (12).

3.2 Unsaturated Zone

In the unsaturated zone of an unconfined aquifer, heat transport is maintained primarily by conduction (9), and can

be described by Fourier's law

$$\frac{\partial}{\partial t}\left(\rho_B C_B T\right) - \frac{\partial}{\partial x_i}\left(\Lambda_{B_{ij}} \frac{\partial T}{\partial x_j}\right) = 0 \qquad (13)$$

The bulk heat capacity and density, as well as the thermal conductivity are functions of the moisture content. The moisture distribution depends, on the other hand, on (a) the thermal field of the unsaturated zone, and (b) on the flow field and thermal field of the saturated zone. Because of these complex relationships, the unsaturated solution also becomes nonlinear.

4. METHOD OF SOLUTION

4.1 Analytical Solutions

Only a few analytical solutions have been found for diffusion-convection problems. In 1961 Ogata and Banks (10) presented a solution for a transient diffusion-convection problem.

Avdonin solved the radial symmetrical problem of the time and distance depending temperature distribution for cold water injection into a hot reservoir (1).

The water temperature at the production well of an injection-production doublet can be calculated as a function of time applying a solution developed by Gringarten and Sauty (5).

All these analytical solutions share the problem of including many simplifications necessary to obtain a solution. The soil and fluid parameters are assumed to be homogeneous, isotropic and constant in the area under consideration. The geometry of the area and the boundary conditions must be simple, hence analytic solutions are not suitable for most practical problems.

4.2 Finite Element Approach

One of the most powerful tools for solving diffusion-convection problems numerically is the Finite Element Method. Fundamental publications on this topic were presented by Smith, Farraday, O'Connor (1973) (13), Segol, Pinder, Gray (1975) (12), and Huyakorn, Taylor (1976) (8), solving the system of nonlinear partial differential equations by applying the Galerkin formulation.

4.2.1 The Flow Portion

Introducing a reference density ρ_o and reference hydraulic head

$$h = \frac{p}{\rho_o g} + z \quad , \tag{14}$$

equation (11) becomes

$$\rho\frac{\rho_o g}{S'}\frac{\partial h}{\partial t} - \frac{\partial}{\partial x_i}\left[\frac{\rho k_{ij}\rho_o g}{\mu}\frac{\partial}{\partial x_j}\left(h + z\frac{\rho-\rho_o}{\rho_o}\right)\right] - \rho Q = 0 \quad , \tag{15}$$

where S' is a storage coefficient describing a relative change of volume due to changes of pressure head and ρQ a source or sink term in the solution area. After discretizing the area, trial solutions for the independent variable are assumed to be of the form

$$h \approx h' = \sum N_J h_J\,(t) \quad . \tag{16}$$

Using the weighted residual approach

$$\int_A W_I r dA = 0 \quad , \tag{17}$$

with W_I as weighting at node I equation (15) can be written as

$$\int_A W_I \left\{\rho\frac{\rho o g}{S'}\frac{\partial h}{\partial t} - \frac{\partial}{\partial x_i}\left[\frac{\rho\rho_o g k_{ij}}{\mu}\frac{\partial}{\partial x_j}\left(h+z\frac{\rho-\rho_o}{\rho_o}\right)\right] - \rho Q\right\} dA = 0 \tag{18}$$

Introducing the trial solution equation (16) and applying Green's theorem, equation (18) becomes

$$\int_A \frac{\rho\rho_o g}{S'} W_I N_J \frac{\partial h_J}{\partial t} dA + \int_A \frac{\rho\rho_o g k_{ij}}{\mu} \frac{\partial W_I}{\partial x_i} \frac{\partial N_J}{\partial x_j} h_J dA$$

$$+ \int_A \frac{\rho\rho_o g k_{ij}}{\mu} \frac{\partial W_I}{\partial x_i} \frac{\rho-\rho_o}{\rho_o} \frac{\partial N_J}{\partial x_j} z_J \, dA \tag{19}$$

$$- \int_S W_I \rho q_n dS' = \int_A W_I \rho Q dA \quad .$$

This approach leads to a linear equation system of the form

$$\left[A\right] \cdot \left\{\frac{\partial h}{\partial t}\right\} + \left[B\right] \left\{h\right\} = \left\{F\right\} \quad , \tag{20}$$

where

$$A_{IJ} = \sum_e \int_A \frac{\rho\rho_o g}{S'} N_I N_J dA \quad , \tag{21}$$

$$B_{IJ} = \sum_e \int_A \frac{\rho\rho_o g}{\mu} k_{ij} \frac{\partial N_I}{\partial x_i} \frac{\partial N_J}{\partial x_j} dA \quad , \tag{22}$$

and

$$F_I = \sum_e \left\{ - \int_A \frac{\rho\rho_o g}{\mu} k_{ij} \frac{\partial N_I}{\partial x_i} \frac{\rho-\rho_o}{\rho_o} \frac{\partial N_J}{\partial x_j} z_J \, dA \right. \tag{23}$$

$$\left. + \int_S W_I \rho q_n dS' + \int_A W_I \rho Q dA \right\} .$$

The weighted finite difference scheme is used for integration with respect to time:

$$\left(\frac{[A]^t}{\Delta t} + \theta [B]^t \right) \{h\}^{t+\Delta t} = \{F\}^t + \left(\frac{[A]^t}{\Delta t} - (1-\theta)[B]^t \right) \{h\}^t \quad . \tag{24}$$

Knowing the pressure distribution of the solution region the mass flux can be calculated from equation (10) and the average fluid velocities from equation (12).

4.2.2 Heat Transport Part

A similar procedure is carried out to solve equation (1) to obtain the temperature distribution in the flow field.

Assuming a trial solution for the unknown temperature

$$T \approx T' = \sum N_J T_J \ (t) \tag{25}$$

and applying the weighted residual approach, one obtains

$$\int_A \frac{\partial}{\partial x_i} \left(D_{ij}, \frac{\partial N_J}{\partial x_j} \right) N_I T_J \, dA \tag{26}$$

$$- \int_A \rho_B C_B N_I N_J \frac{\partial T_J}{\partial t} \, dA \tag{27}$$

$$- \int_A \frac{\partial}{\partial x_i} \rho_F C_F \, (V_i N_J) \, N_I T_J \, dA = 0 \quad . \tag{28}$$

The resulting system of linear equations can be written in matrix form as

$$\left[A\right] \left\{\frac{\partial T}{\partial t}\right\} + \left[B\right]\left\{T\right\} = \left\{F\right\} \quad , \tag{29}$$

where

$$A_{IJ} = \sum_e \int_A \rho_B C_B \, N_I N_J \, dA \quad , \tag{30}$$

$$B_{IJ} = \sum_e \int_A \left(D_{ij}, \frac{\partial N_J}{\partial x_i} \frac{\partial N_I}{\partial x_j} + (\rho_F C_F) \, v_i N_I \frac{\partial N_J}{\partial x_i} \right. \tag{31}$$

$$\left. + (\rho_F C_F \frac{\partial v_i}{\partial x_i}) \right) dA \quad ,$$

and

$$F_I = \sum_e \int_S \left(D_{ij}' N_I \frac{\partial}{\partial x_j} \sum_{m=1}^{n} (T_m N_m) \right) n \, dS' \quad . \tag{32}$$

The same difference scheme as in the flow part is used to approximate the time derivatives.

4.2.3 Free Surface Boundary Condition

The boundary at the free surface of an unconfined aquifer is described by

$$\rho = 0 \tag{33}$$

and

$$\left\{ v \right\}^T \cdot \left\{ n \right\} = 0 \quad , \tag{34}$$

which means that there can be no flux across the surface and the pressure is atmospheric.

At the beginning of a timestep calculation , the position of the free surface is unknown and therefore the boundary condition will not be satisfied. The trial fixed surface will be corrected by a corresponding shift of the node position with a deformation of the elements. This shifting is illustrated by Figure 9 for quadrilateral elements in a vertical cross-section. The process is repeated until satisfactory accuracy is reached.

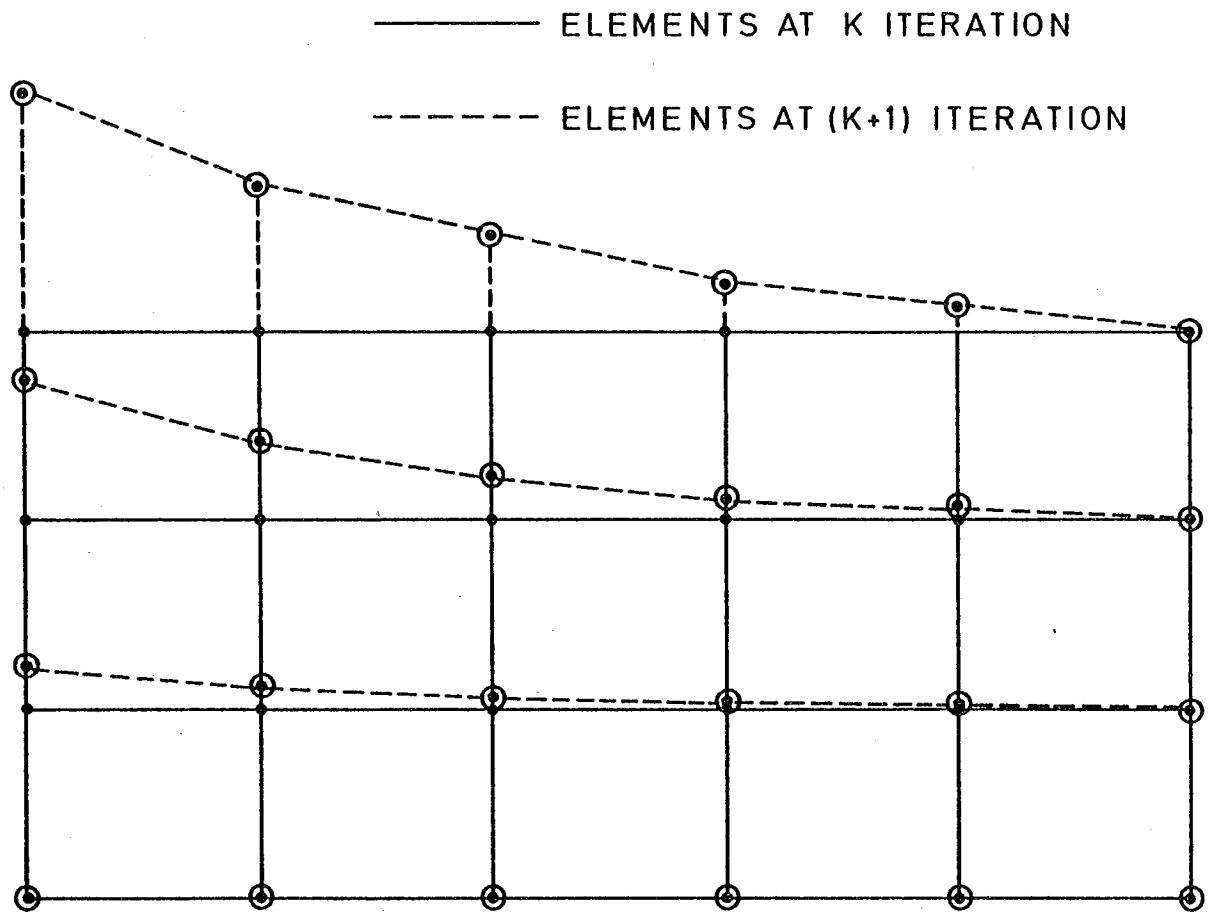

Figure 9. Iteration of the free surface by node shifting.
XBL 808-11159

4.2.4 Heat Transport in the Unsaturated Zone

The discretization for the solution of the heat transport equation is identical to the mesh used for the solution of the flow equation up to the surface. This mesh is complemented by a mesh covering the unsaturated zone from the free surface to the ground surface. Also, this part of the mesh deforms during the iteration process for the determination of the free surface. Figure 10 shows the flow and heat transport meshes at two different iteration steps.

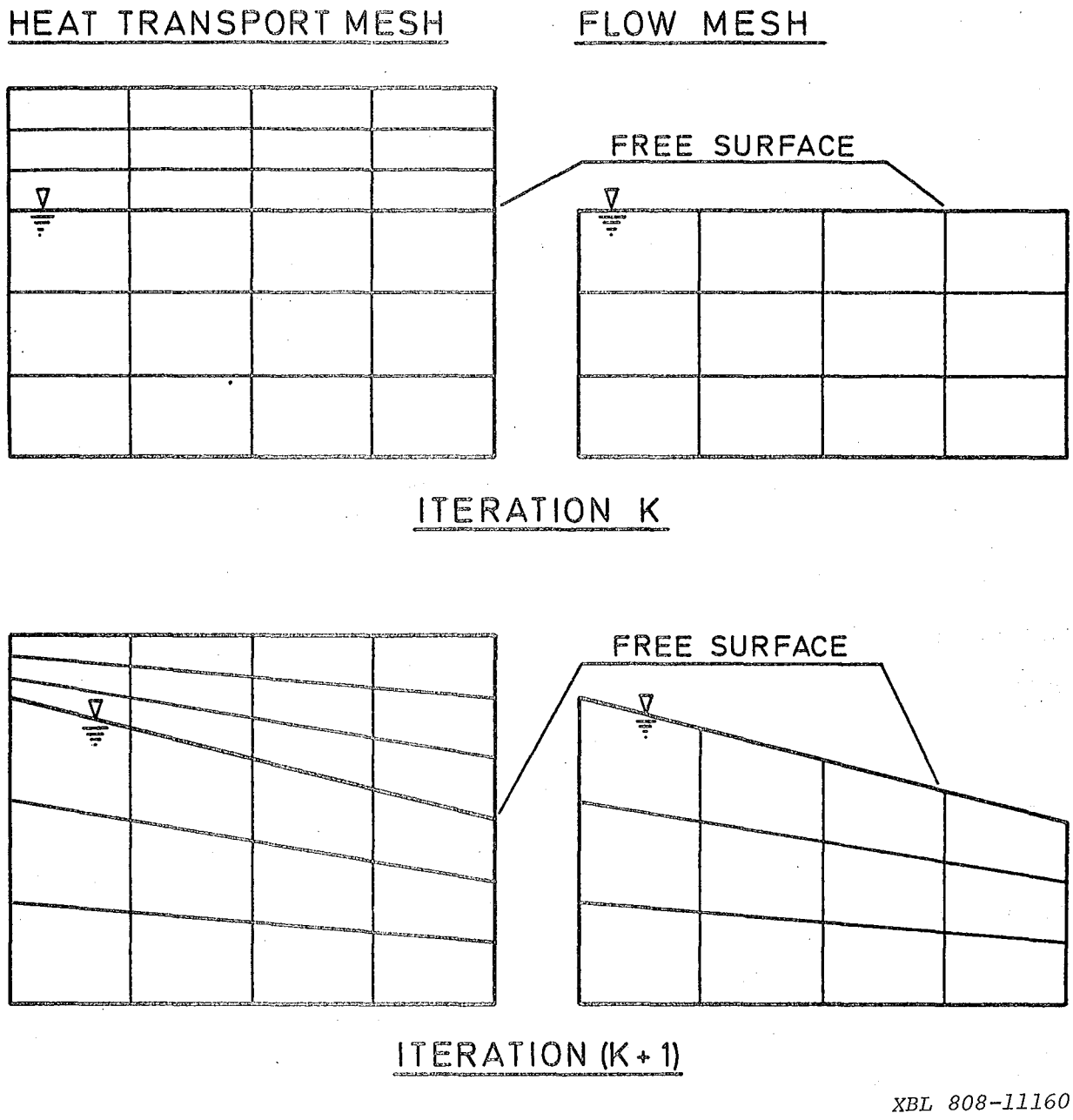

Figure 10. Deformation of heat transport mesh and flow mesh during the iterative calculation of the free surface.

Bulk heat capacity, density, and thermal conductivity of the unsaturated zone are functions of the moisture content. Knowing the free surface, the moisture distribution between

water level and ground surface is calculated by means of an analytical solution (9).

The thermal properties of the elements in the unsaturated zone were determined as functions of the average moisture content in the corresponding element. The fluid velocity in the elements above the water level is zero and the heat transport equation can be solved.

4.2.5 Treatment of the Nonlinearities

The differential equations which must be solved to calculate the temperature field of flowing groundwater in a shallow aquifer with free surface are highly nonlinear. Different iterative solutions become necessary on several levels in the solution procedure, illustrated by the flow chart in Figure 11.

Starting the calculation at a new time step, the temperature, pressure, and velocity distributions of the previous timestep are known and regarded as an approximation of the solution for the timestep under consideration. The flow parameters are calculated as functions of the temperature field, and the equation system is assembled. Introducing the boundary conditions, the equation system can be solved. If the resulting pressure distribution does not satisfy the free surface boundary condition, the nodes are shifted as described above and a new flow calculation executed. If the free surface boundary condition is satisfied, the moisture distribution of the unsaturated zone is calculated.

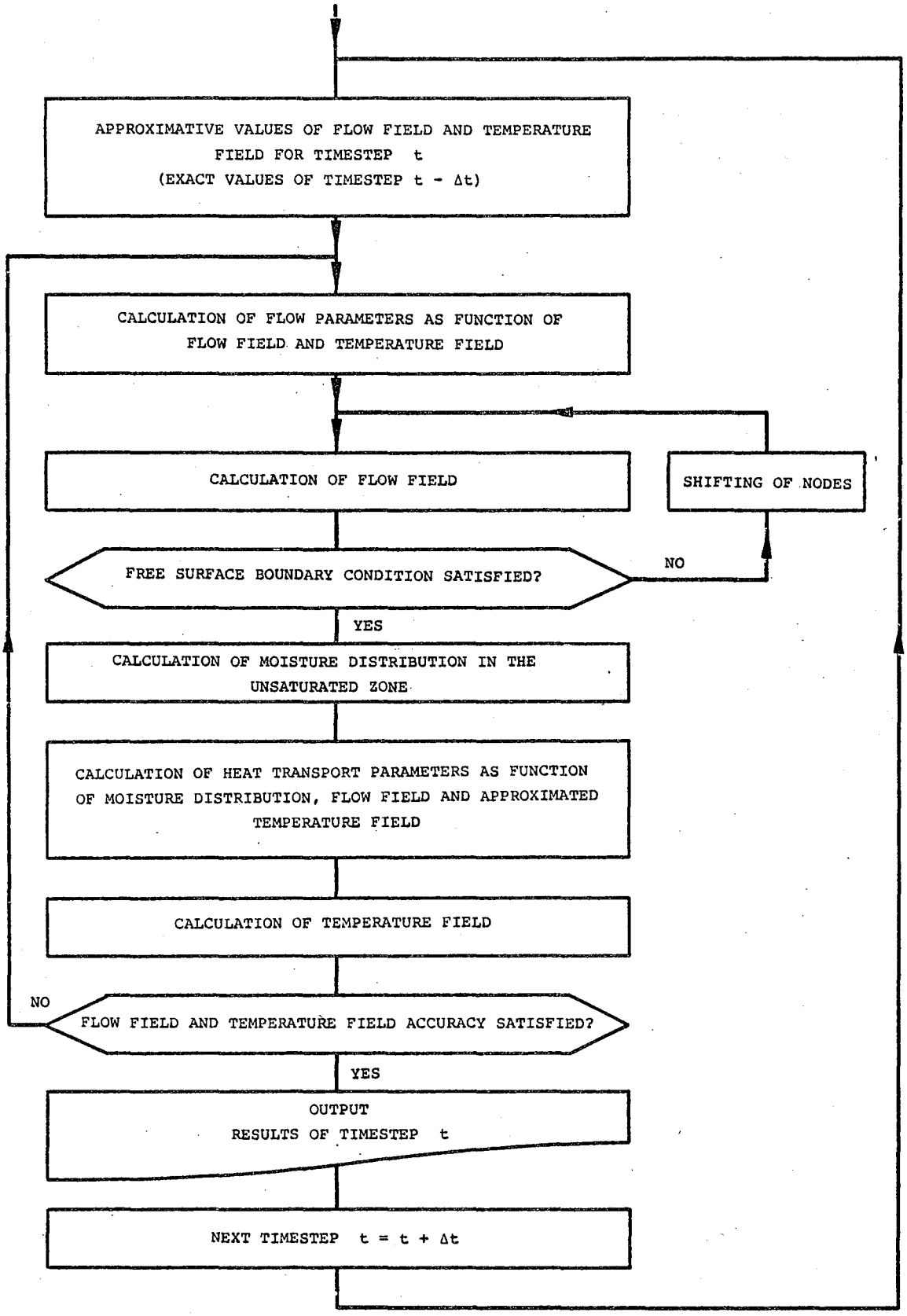

Figure 11. Flow chart of iterative calculations. *XBL 808-11161*

The heat transport parameters which are functions of the flow field, moisture content, and temperature distribution can be calculated and the equation system will be assembled. The solution vector of this linear equation system is the temperature distribution in the solution region.

If the required accuracy is not achieved, a new iteration step has to be done, starting with updated flow parameters that depend on the computed flow and temperature distributions. If the accuracy is sufficient, the results can be printed and the calculation will continue with the next timestep.

If only small changes of the parameters are considered, a time-lagged coupling of the equations by updating the parameters only once at each timestep may yield satisfactory results and thus save computing time.

5. EXAMPLES FOR TWO WELL STORAGE SYSTEMS

The application of two well storage systems for space heating and air conditioning may be illustrated by a hypothetical example based on realistic aquifer parameters and climatic data valid for a region near Boston, Massachusetts (4).

5.1 Meteorological Data

The average temperature distribution for the period of one year is shown in Figure 12. A maximum average daily temperature of 24.4°C occurs in July, a minimum of -1.1°C in January and February. The yearly average air temperature is 11.25°C. Due to the positive radiation balance and the geothermal heat flux the average groundwater temperature is 12.0°C.

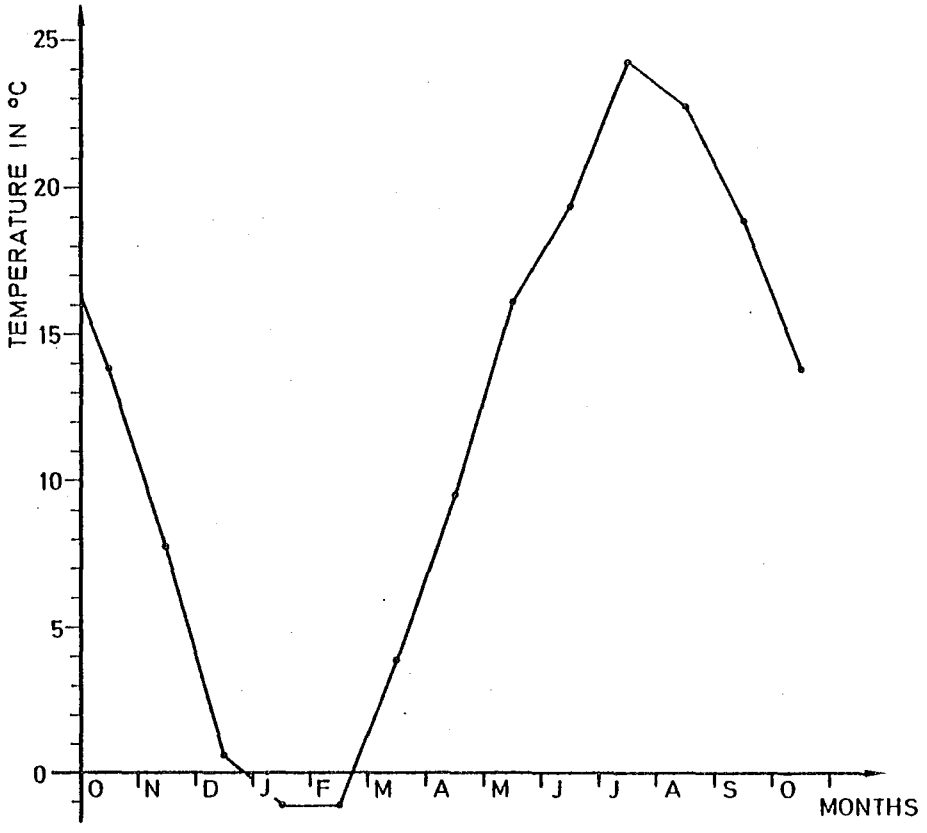

Figure 12. Temperature distribution over one year (daily averages). *XBL 808-11162*

5.2 Aquifer Data

Figure 13 shows a vertical profile of the aquifer under consideration. The natural hydraulic gradient is very small and the resulting fluid velocities negligible. The unconfined aquifer's free surface is 6.0 m below the ground surface and the saturated zone is 25.0 m thick.

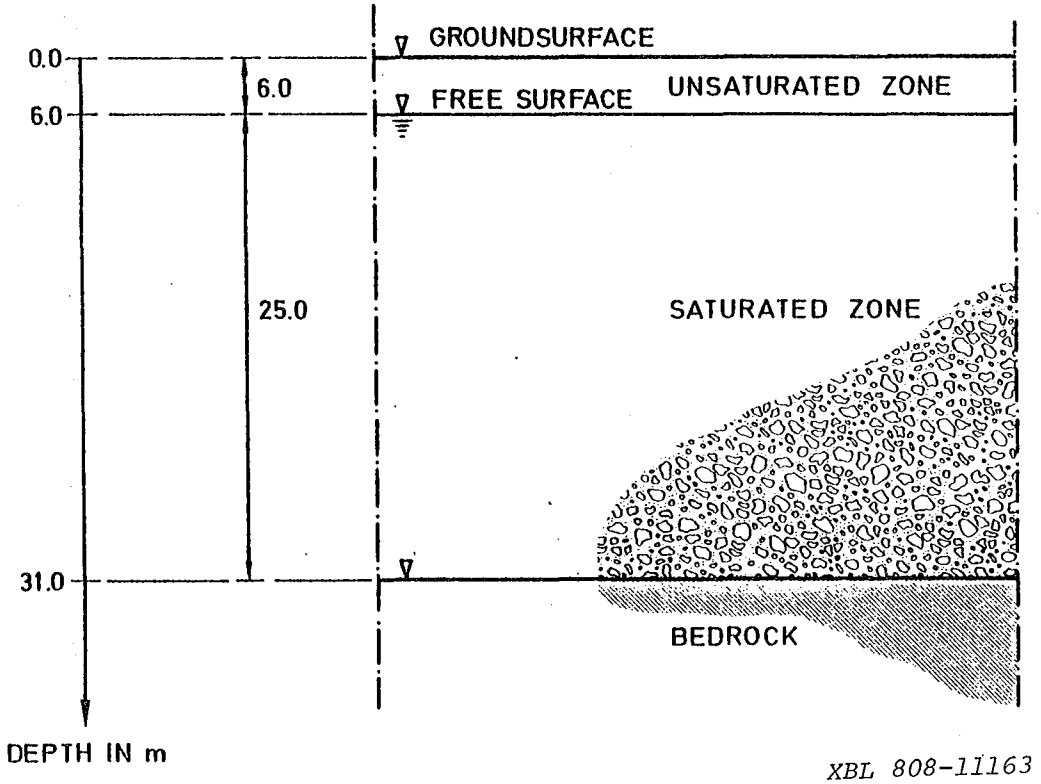

Figure 13. Vertical cross-section of the aquifer.

The other aquifer properties are summarized in Table 1, Table 2, and Table 3.

Table 1: Bedrock properties		
Hydraulic permeability	$1.0 \cdot 10^{-16}$	m^2
Porosity	0.15	---
Storage coefficient	$1.0 \cdot 10^{-5}$	---
Density	2500.0	$Kg \cdot m^{-3}$
Longitudinal dispersion factor	66.0	m
Transversal dispersion factor	6.60	m
Thermal conductivity	2.80	$W \cdot m^{-1} \cdot {}^{o}C^{-1}$
Heat capacity	980.0	$J \cdot Kg^{-1} \cdot {}^{o}C^{-1}$

Table 2: Solid matrix properties of aquifer		
Hydraulic permeability	$1.0 \cdot 10^{-12}$	m^2
Porosity	0.25	---
Effective porosity	0.23	---
Density	2500.0	$Kg \cdot m^{-3}$
Longitudinal dispersion factor	66.0	m
Transversal dispersion factor	6.60	m
Thermal conductivity	2.5	$W \cdot m^{-1} \cdot {}^{o}C^{-1}$
Heat capacity	950.0	$J \cdot Kg^{-1} \cdot {}^{o}C^{-1}$

Table 3: Fluid properties		
Reference density	1000.0	$Kg \cdot m^{-3}$
Reference conductivity	0.5254	$W \cdot m^{-1} \cdot {}^{o}C^{-1}$
Reference heat capacity	4200.0	$J \cdot Kg^{-1} \cdot {}^{o}C^{-1}$
Reference dynamic viscosity	$1.792 \cdot 10^{-5}$	$Kg \cdot m^{-1} \cdot s^{-1}$

5.3 Numerical Calculations

The numerical calculations for this report were carried out with the program FETCH developed at LBL in 1980 (6). It is based on the Finite Element Method described above. For the discretization of the solution region isoparametric quadrilateral elements are used.

Due to the negligible natural fluid velocity in the aquifer under consideration, a three-dimensional axisymmetric discretization was chosen. The vertical profiles of the flow and heat transport meshes are shown in Figure 14. The flow mesh consists of 243 nodes and 208 elements. The heat transport mesh is identical to the flow mesh up to the free surface. The extension through the unsaturated zone to the groundsurface increases the number of nodes and elements by 81, 78 respectively, so that the heat transport mesh consists of 324 nodes and 286 elements. The meshes are comparatively fine in regions of maximum expected gradient (thermal or hydraulic), i.e., near the production or recharge well for both meshes and in the unsaturated zone for the heat flux mesh.

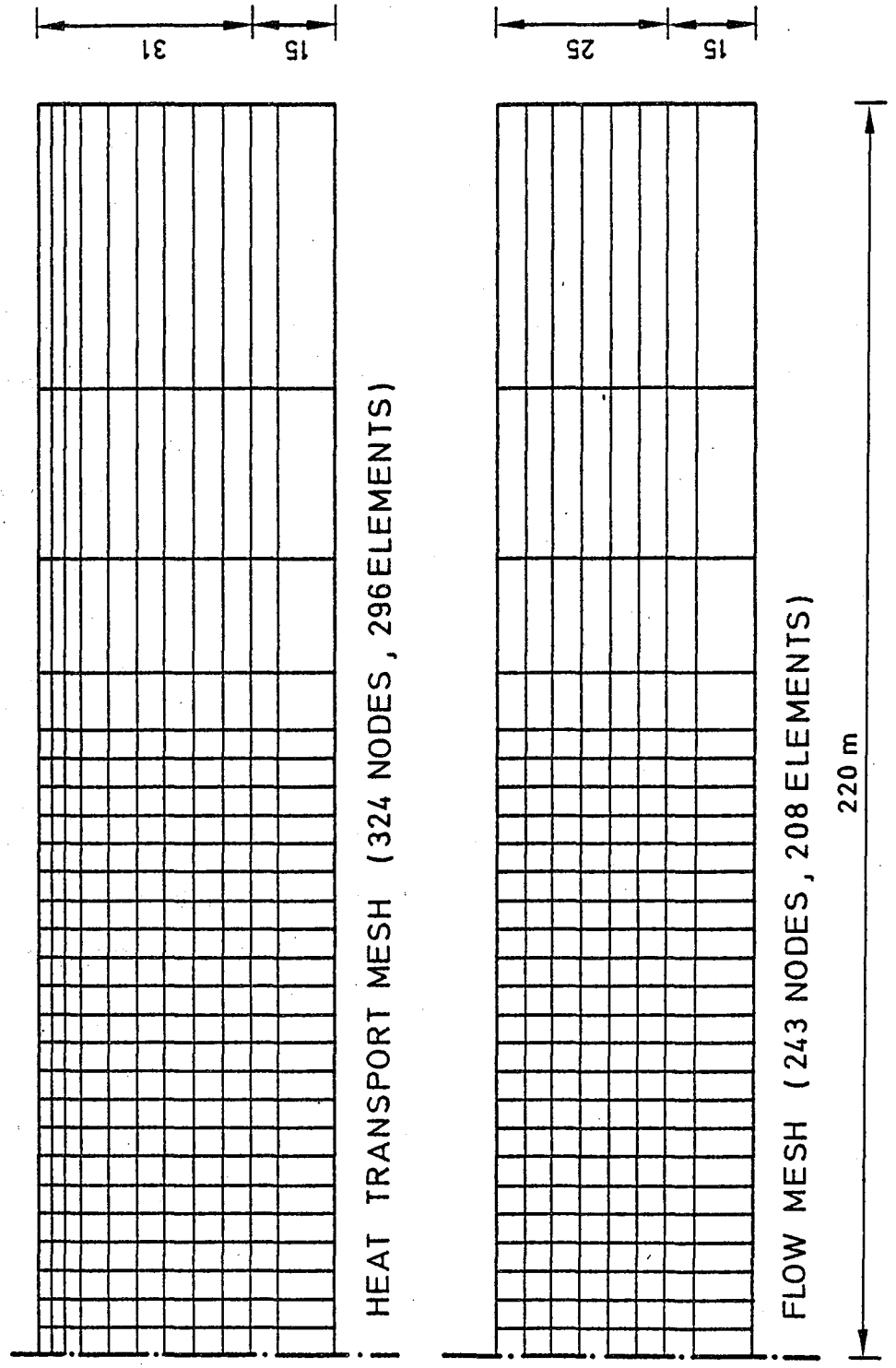

XBL 808-11175

Figure 14. Meshes for flow and heat transport calculation.

5.4 Natural Soil Temperature Distribution

5.4.1 Problem

The temperature of the groundwater in most situations is reasonably stable, but there is still some response to the variations in air and ground surface temperature (see Figure 2 and Figure 3). Under normal circumstances the penetration of the temperature fluctuation induced by diurnally varying surface temperatures is negligible. Seasonal variations, on the other hand, are measurable at greater depth and require consideration.

The seasonal temperature changes for the aquifer are calculated in the following based on existing meteorological data and the aquifer parameters of Table 1, Table 2, and Table 3.

5.4.2 Boundary Conditions

The flow boundary conditions are shown in Figure 15a. Since there is no pumping or recharge in the solution area for this case, the left, right, and lower boundaries are impermeable. The upper boundary is the free surface, which is not changing position in this calculation.

In Figure 15b the heat transport boundary conditions are illustrated. The temperature at the lower boundary is a time-independent Dirichlet condition, while the upper boundary is a time-dependent Dirichlet condition, because the surface temperature changes with time. The right and left vertical boundaries are impermeable.

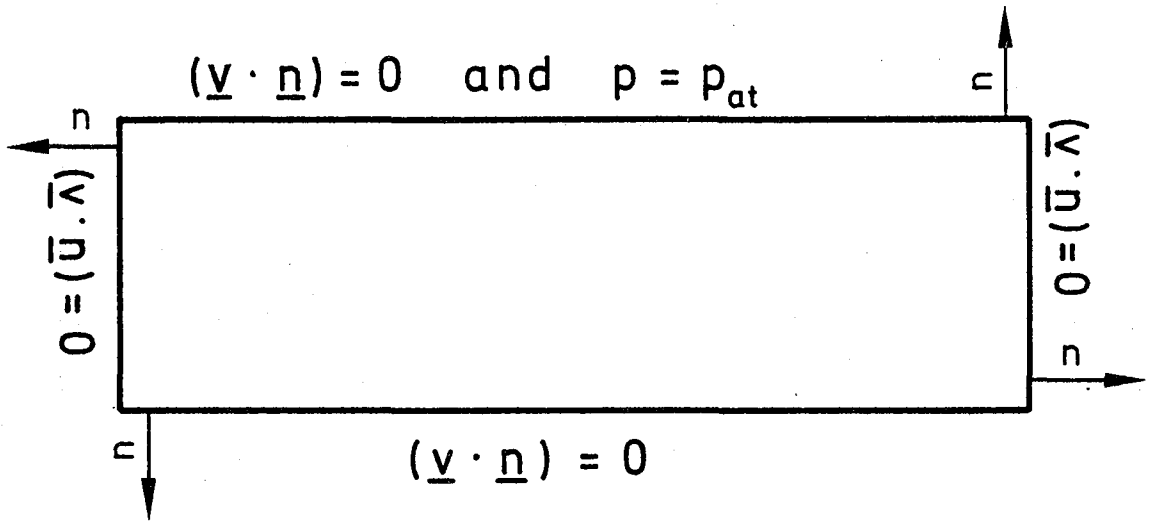

Figure 15a. Flow boundary conditions.

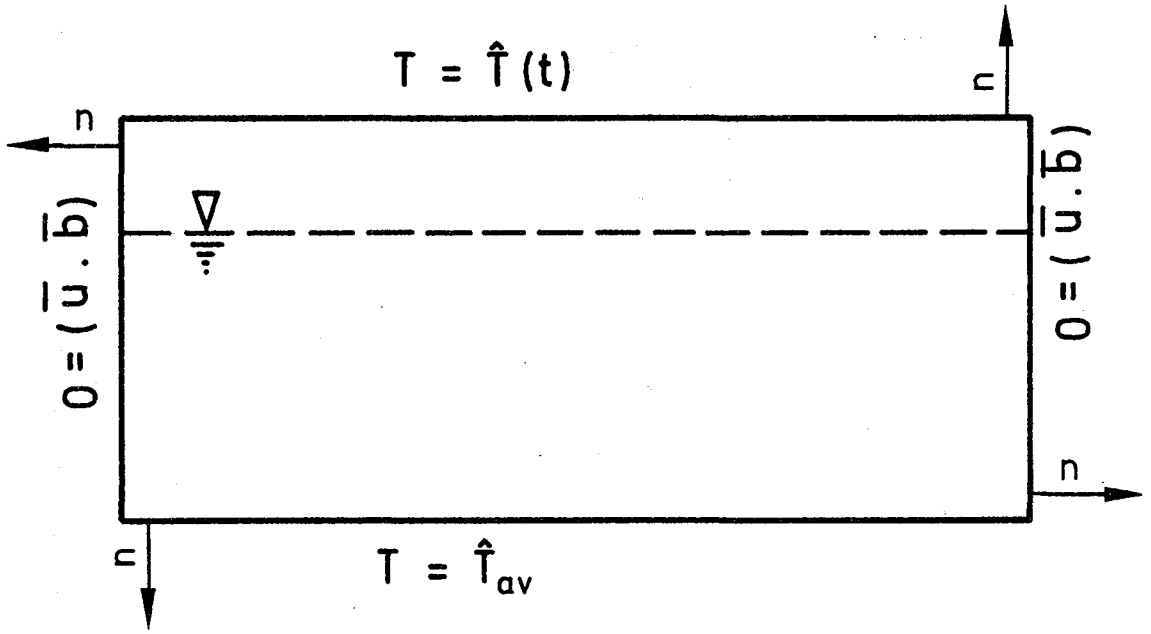

Figure 15b. Heat transport boundary conditions. *XBL 808-11164*

5.4.3 Results

The temperature changes at the surface are greatly attenuated as they penetrate the ground. Distributions for different seasons are shown in Figure 16, and Figure 17 presents the seasonal variations of the soil and groundwater temperature at different depths below the surface. Since the temperature gradients are very small, no significant density differences occur and density-induced flow could not be observed.

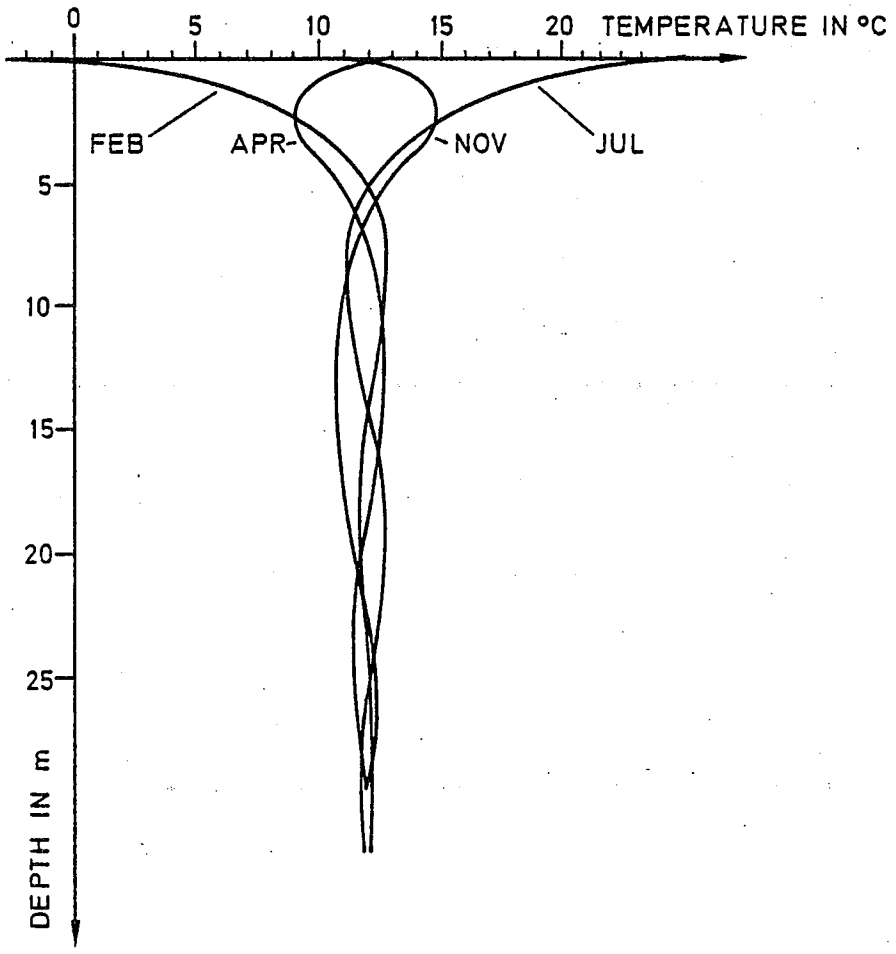

XBL 808-11165

Figure 16. Calculated seasonal temperature distributions in the aquifer as function of depth below the surface.

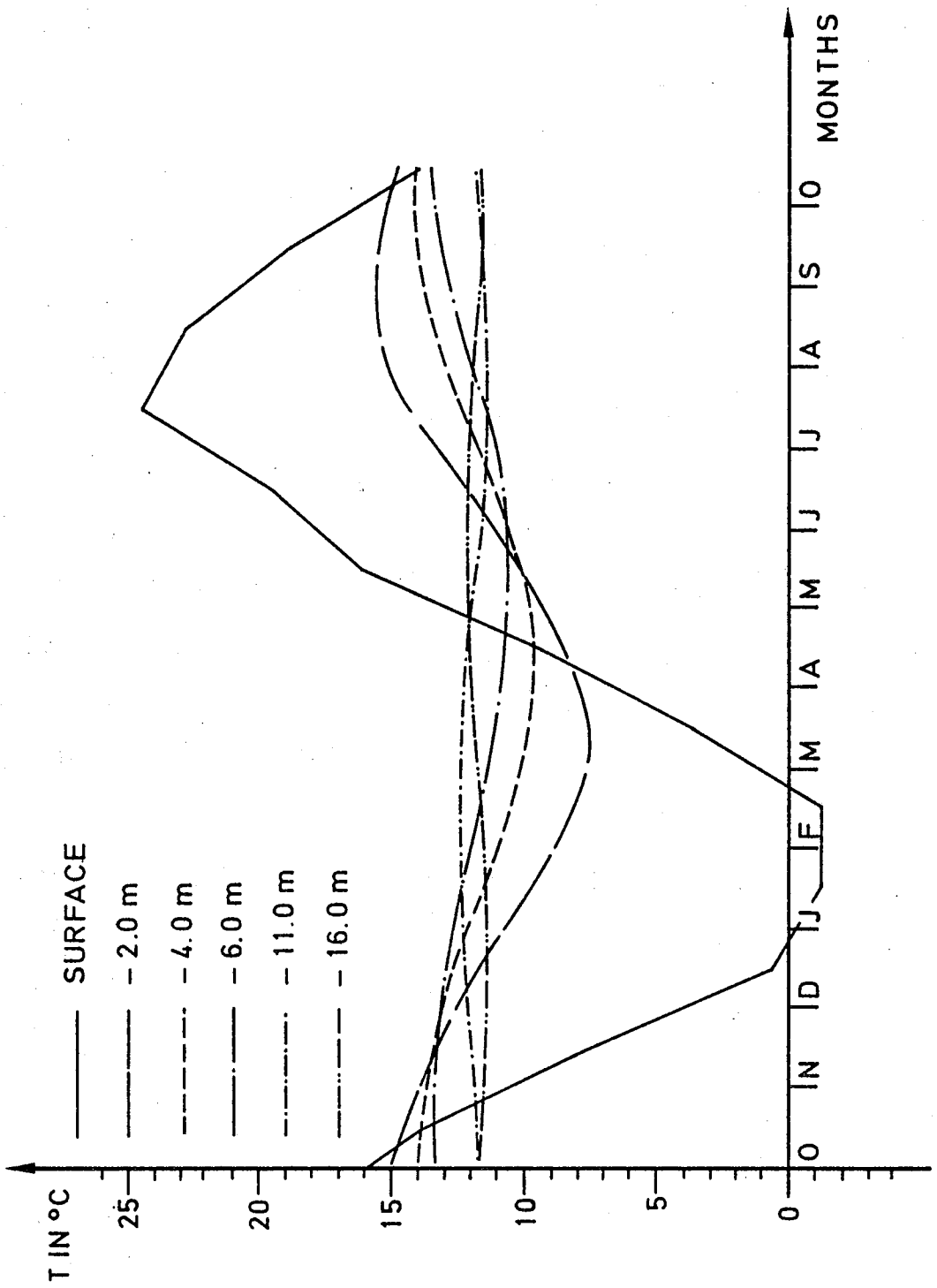

XBL 808-11176

Figure 17. Calculated seasonal changes of soil and groundwater temperatures in different depths below the surface.

5.5 Cold Water Storage

The aquifer described above will be used as an energy source for space heating and air conditioning by means of a two well storage system illustrated in Figure 7. In winter groundwater is extracted from the warm water well. The water has the natural groundwater temperature and is led to the water source heat pump where part of its energy content is transferred to the heating system. The water is cooled by about $6^{\circ}C$ and reinjected into the aquifer by means of the cold water well. In summer, when air conditioning is required, water is pumped from the cold water well to the heat pump. This water is colder than the natural groundwater temperature and can remove more heat from the cooling system. This process warms the water up to the natural groundwater temperature, whereupon it is recharged through the warm water well into the aquifer.

Figure 18 shows the heating/cooling demand of 750 families, living in multi-family-apartment-houses, under climatic conditions as described above. The energy demand of each apartment depends on its position in the house, its area, etc.

For the calculation of the energy demand of an average apartment the following assumptions were made (4):

1. The walls and the roofs of the apartment houses are well insulated.
2. Every unit is inhabited by two adults and two children.
3. 0.25 air changes per hour are required.
4. Size of average apartment as shown in Table 4.

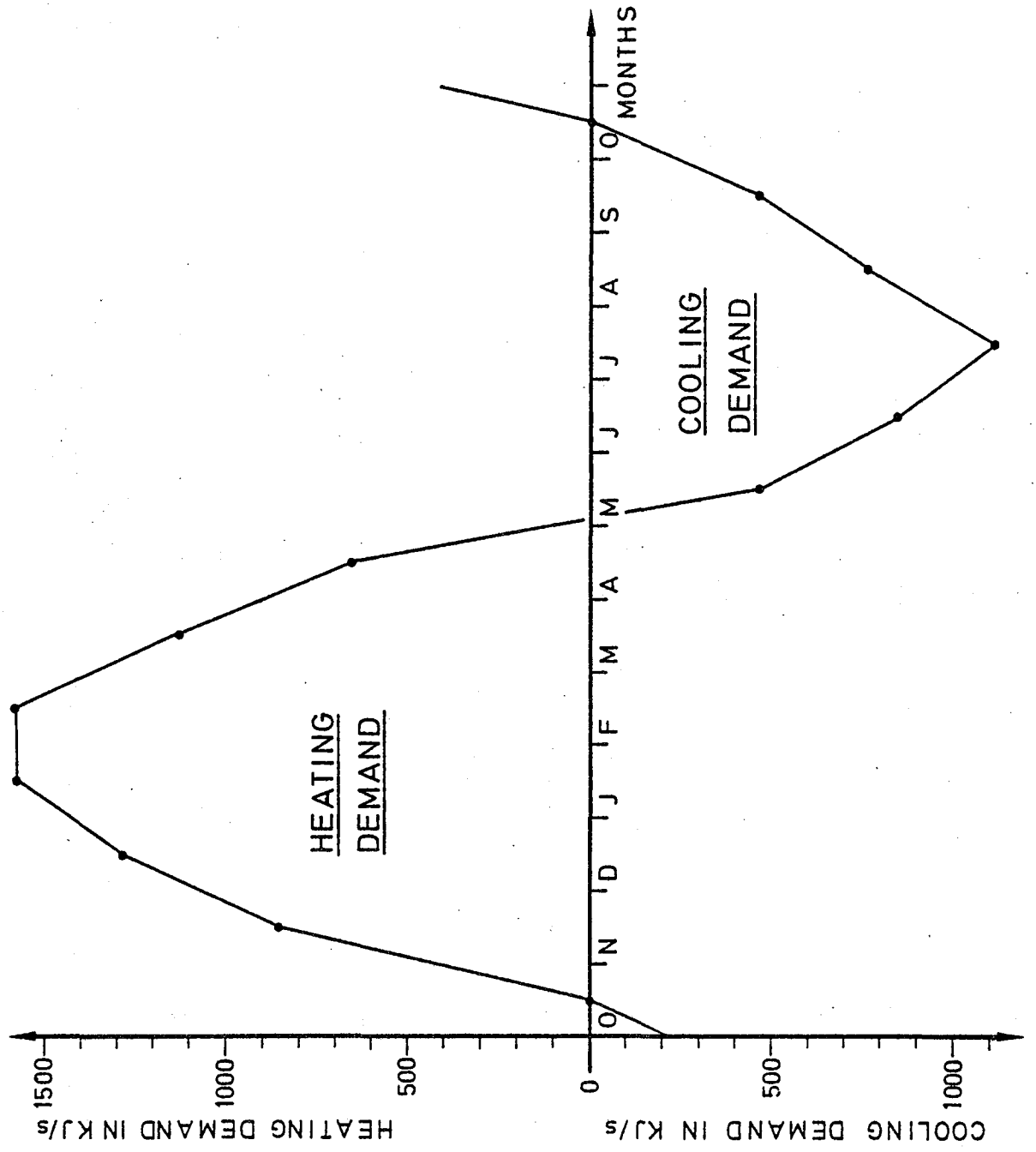

XBL 808-11177

Figure 18. Heating and cooling demand for 750 families.

Table 4: Size of an average apartment		
Floor area	100.0	m^2
Exterior walls	35.0	m^2
Interior corridor walls	25.0	m^2
Roof area (proportionate)	35.0	m^2

Since the recharge into the aquifer at the warm water well is in this case at the same temperature as the natural groundwater temperature of the aquifer, no changes of the temperature field occur around this well and only the observation of the cold water well is necessary.

5.5.2 Boundary Conditions

The reliability of the calculation depends strongly on the accuracy of the description of the boundary conditions. The flow field is described by an impermeable lower boundary and a constant pressure boundary condition on the circumference. The solution of the free surface problem is the same as described above.

The hydraulic and thermal description of the well is much more complicated, since not only does the value of the boundary condition change with time, but the type of boundary condition changes also.

During the injection period, the temperature and the mass

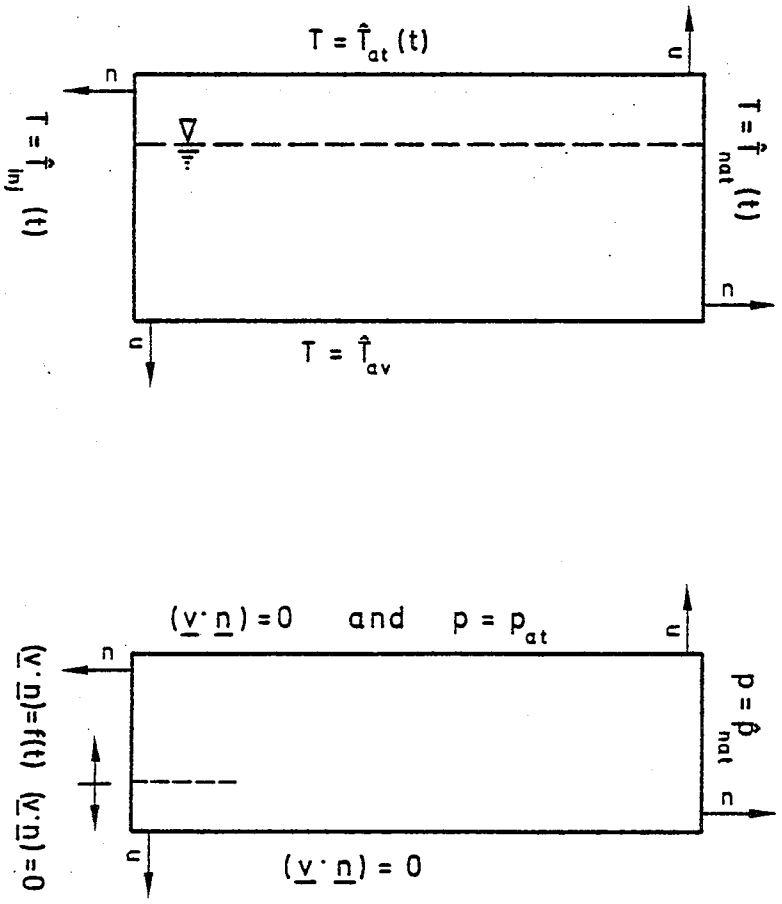

XBL 808-11178

Figure 19. Cold water well injection - Boundary conditions.

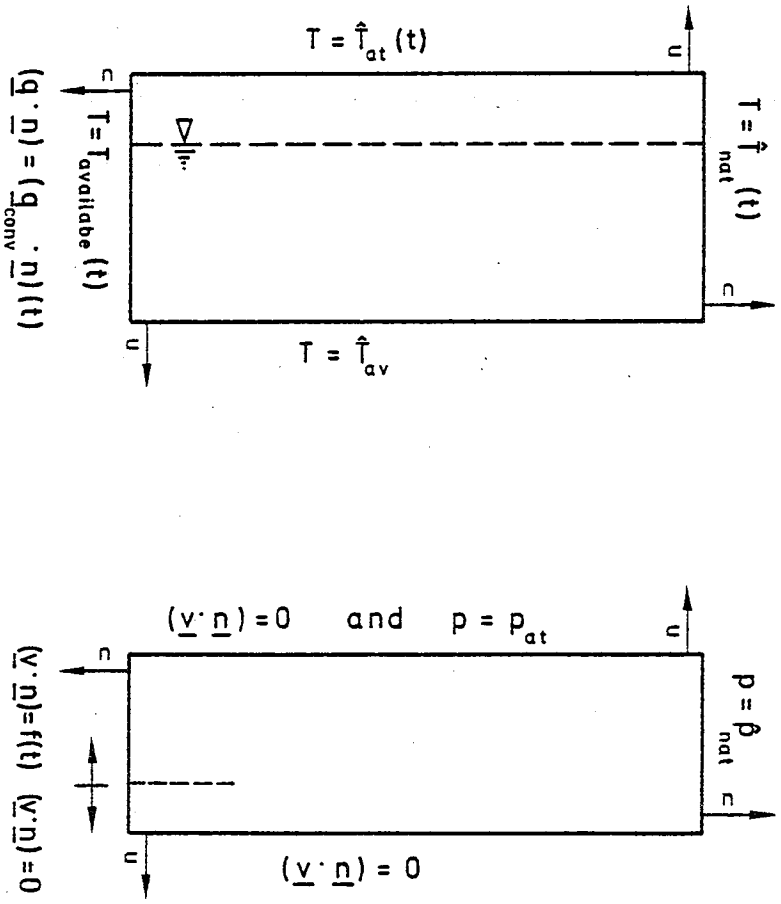

XBL 808-11179

Figure 20. Cold water well extraction - Boundary conditions.

flux of the injected water is known, so that the temperature field can be described by a time-dependent Dirichlet condition and the flow field by a time-dependent Neumann condition.

For the extraction period only the cooling demand and the desired reinjection temperature is known. The temperature at which the water can be extracted is unknown and depends also on the extraction history.

The mass flux must be adjusted to satisfy the respective cooling demand, and is described as an iteratively determined time-dependent Neumann condition. Starting with an estimated mass flux for the time interval under consideration, the cooling capacity is calculated by means of this flux and the resulting available temperature. Comparison with the actual cooling demand yields a correction of the mass flux and a new calculation of the timestep. This iterative process is carried out until a satisfactory agreement between cooling demand and cooling capacity is reached for the timestep.

In this iterative process the temperature field boundary condition is described as an iteratively determined time-dependent Neumann condition, which allows convective heat flux only and prevents conductive heat transport. The upper Dirichlet condition of the thermal field at the surface changes its temperature with the ground surface temperature.

The peripheral boundary is described as a time-dependent Dirichlet condition by the corresponding natural temperature distribution for each timestep calculated in 5.4. The lower boundary is assumed to be isothermal.

5.5.3 Results

Three injection/extraction cycles were calculated, covering a total time of three years. Surface temperature changes, natural groundwater temperature distribution and cooling/heating demand are assumed to be the same in all three years. Figure 21 shows the mass flux in the well for the first year, including the iteratively determined fluxes during the extraction period and the assumed mass fluxes based on an estimated linear relation between extraction temperature and time.

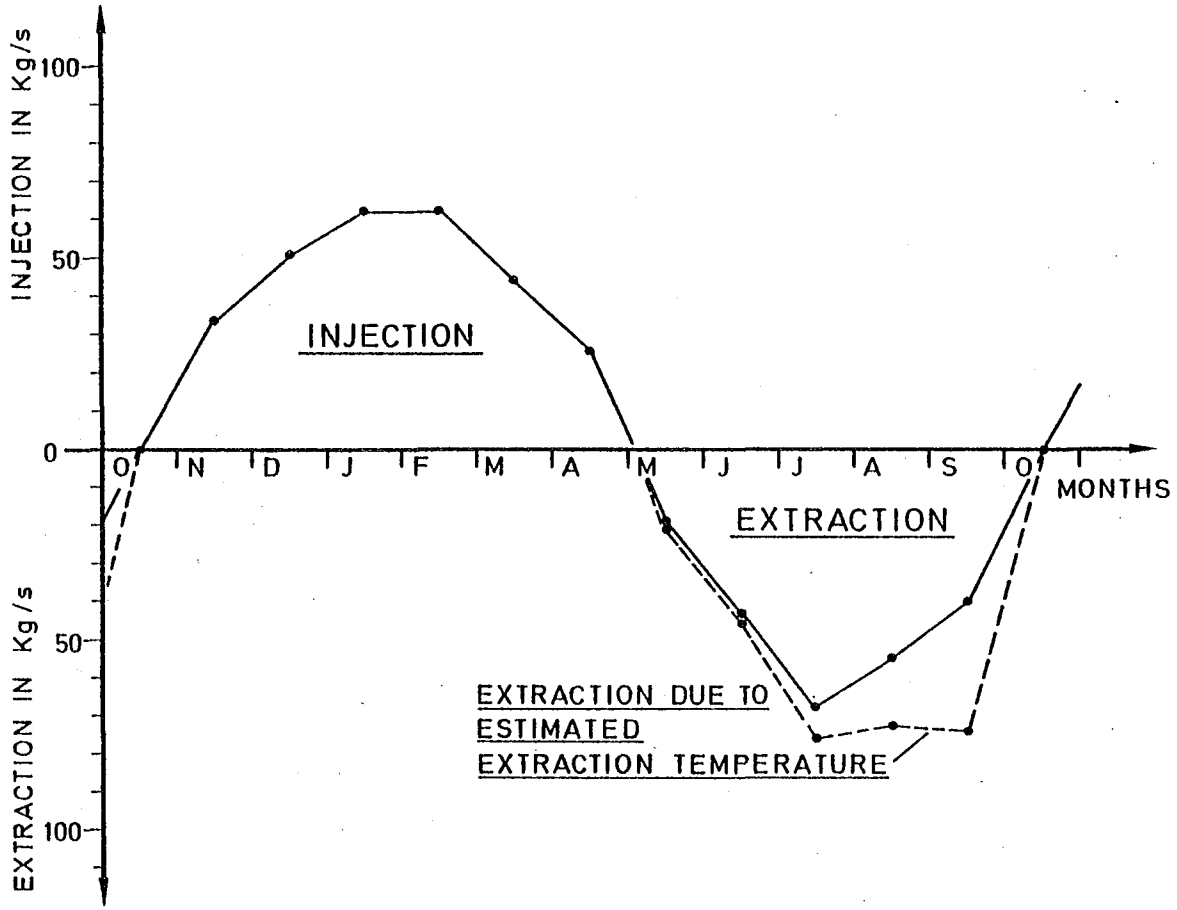

XBL 808-11166

Figure 21. Calculated and estimated mass flow (first cycle).

The total amount of additionally injected cooling capacity is 18.03 TJ. The recovering factor, defined as quotient of extractable cooling (or heating) capacity and injected cooling (or heating) capacity depends on many different parameters, such as geological and meteorological data, and is a function of the extraction history. Figure 22 shows the recovery factor as a function of time for the first extraction cycle.

Since the cooling demand is smaller than the heating demand, for the conditions of this example, the extraction was not to be continued until the recovery factor approached zero.

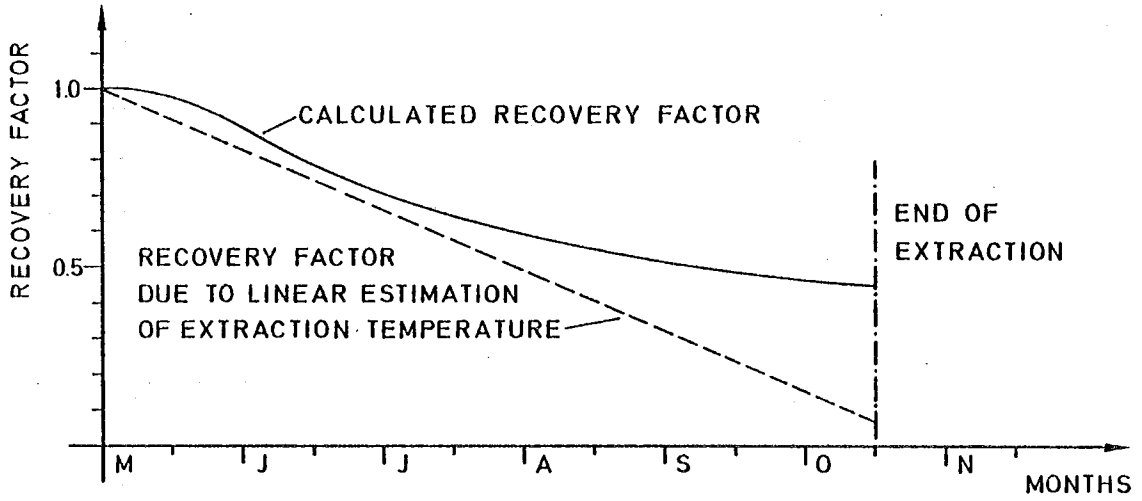

Figure 22. Estimated and calculated recovery factor. *XBL 808-11167*

715.4 Gg water with a total cooling capacity of 18.03 TJ were injected and 566.3 Gg must be extracted to satisfy a total cooling demand of 9.06 TJ, which leads to an overall recovery factor of about 0.64. This overall recovery factor increases from cycle to cycle as can be seen in Figure 23,

which shows the available extraction temperature for all three years.

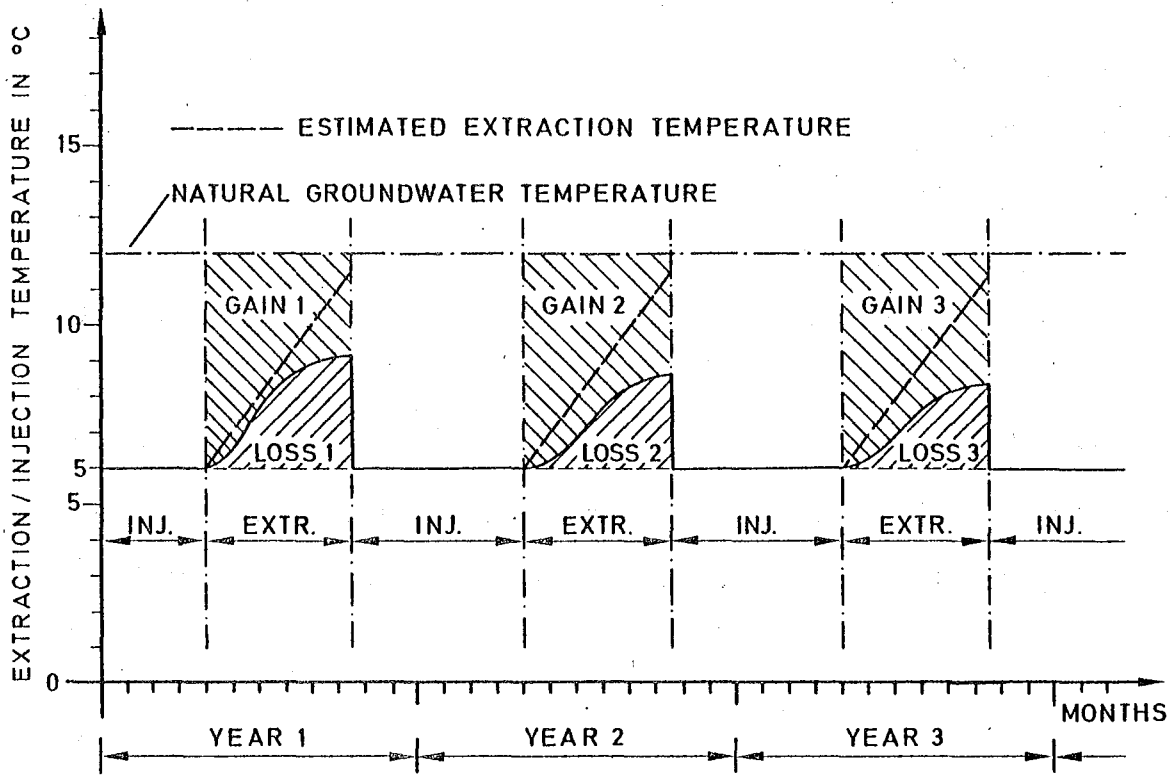

Figure 23. Available extraction temperatures. *XBL 808-11168*

The horizontal expansion of the temperature anomaly can be seen in Figure 24 in which the vertical mean temperatures of the saturated zone are plotted against the radius for several characteristic times. It is obvious that the radius of the influenced area changes insignificantly after two or three injection/extraction cycles. This fact can also be seen in Figure 25, where the vertical temperature distribution of the aquifer is plotted for different radii and timesteps. The

differences between the temperature profiles of the second and third cycle are small.

In spite of the decreasing heat conductivity in the unsaturated zone, the temperature changes above the free surface are significant. The temperature gradients are changing in magnitude and direction. The heat fluxes between the surface and deeper layers are interrupted leading to an overall decrease in the temperatures of the aquifer.

Due to the reasonable small temperature difference between the injected water and the average aquifer temperature at the cold water well and no temperature differences at the warm water well, a minimum of negative influences on the environment can be expected by applying this system of two-well storage.

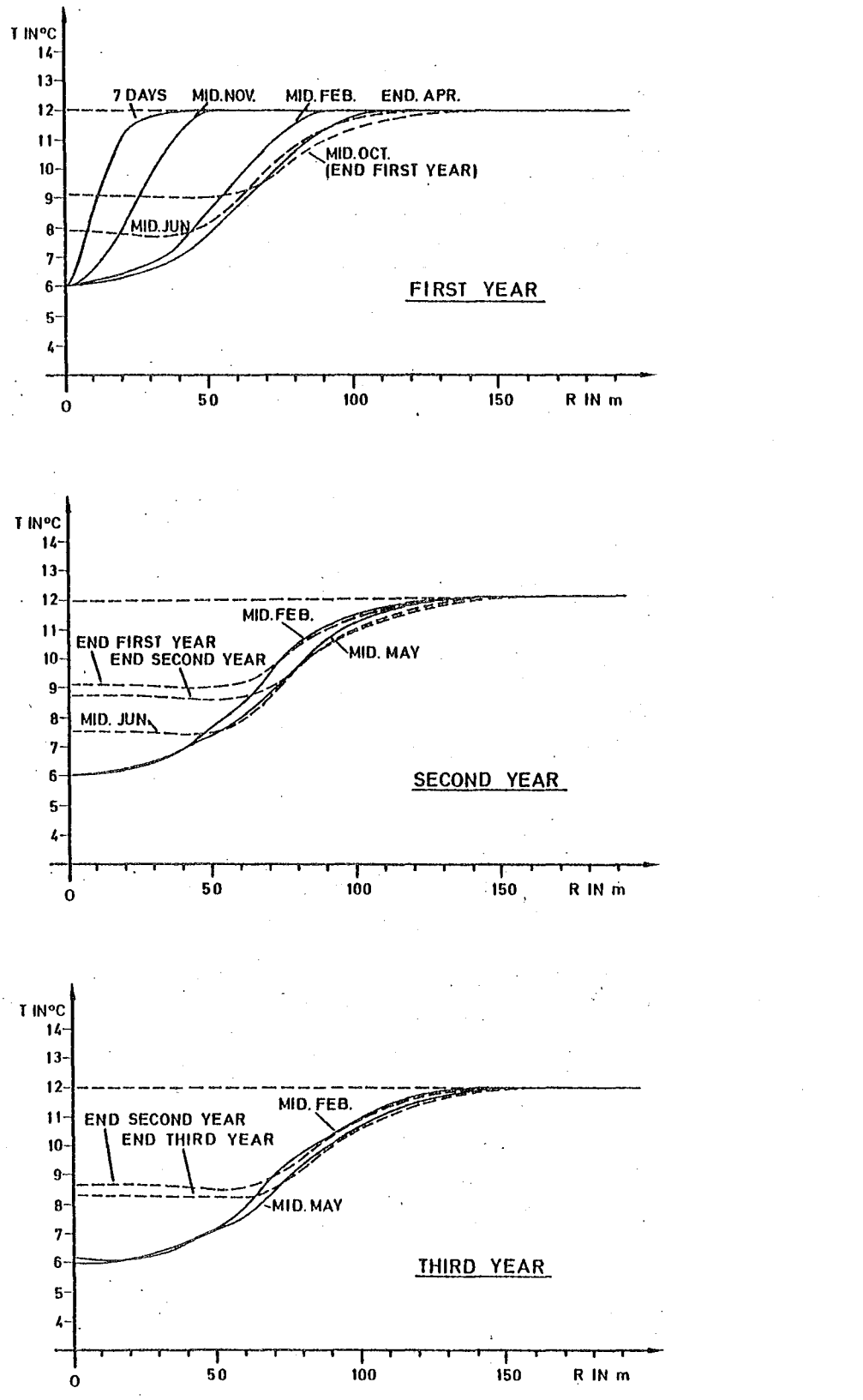

XBL 808-11169

Figure 24. Average temperature of the aquifer versus radius.

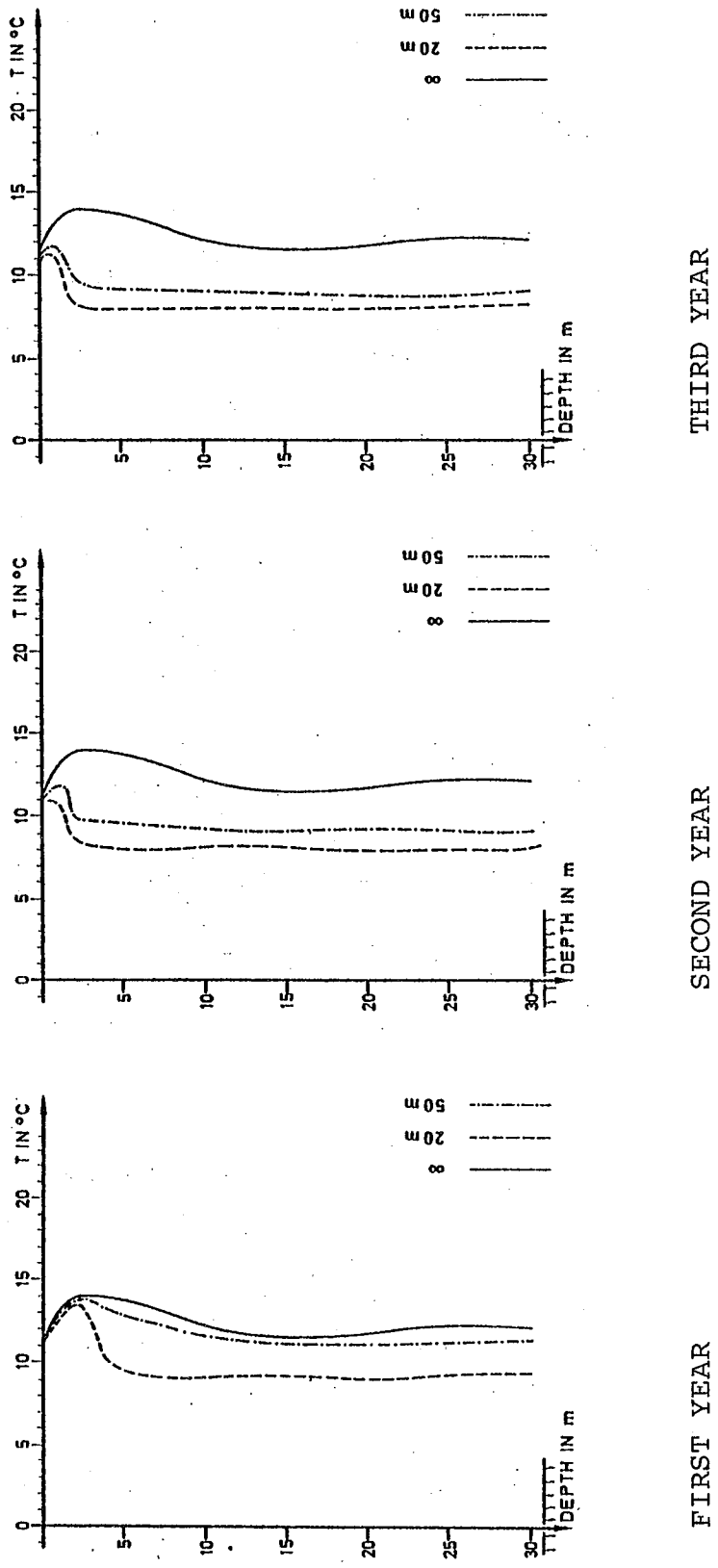

XBL 808-11180

Figure 25a. Temperature distribution in vertical cross-sections (November 1).

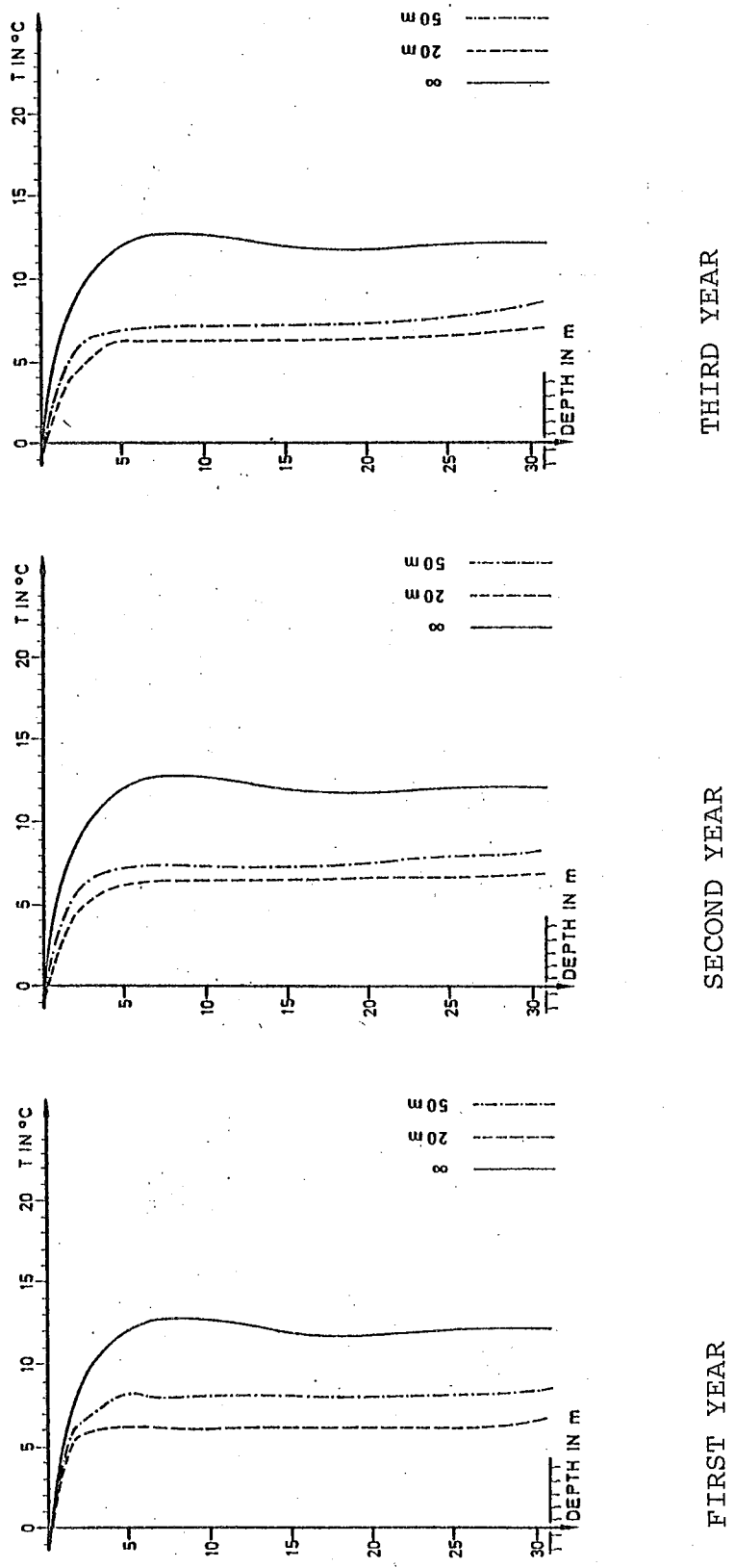

XBL 808-11181

Figure 25b. Temperature distribution in vertical cross-sections (February 1).

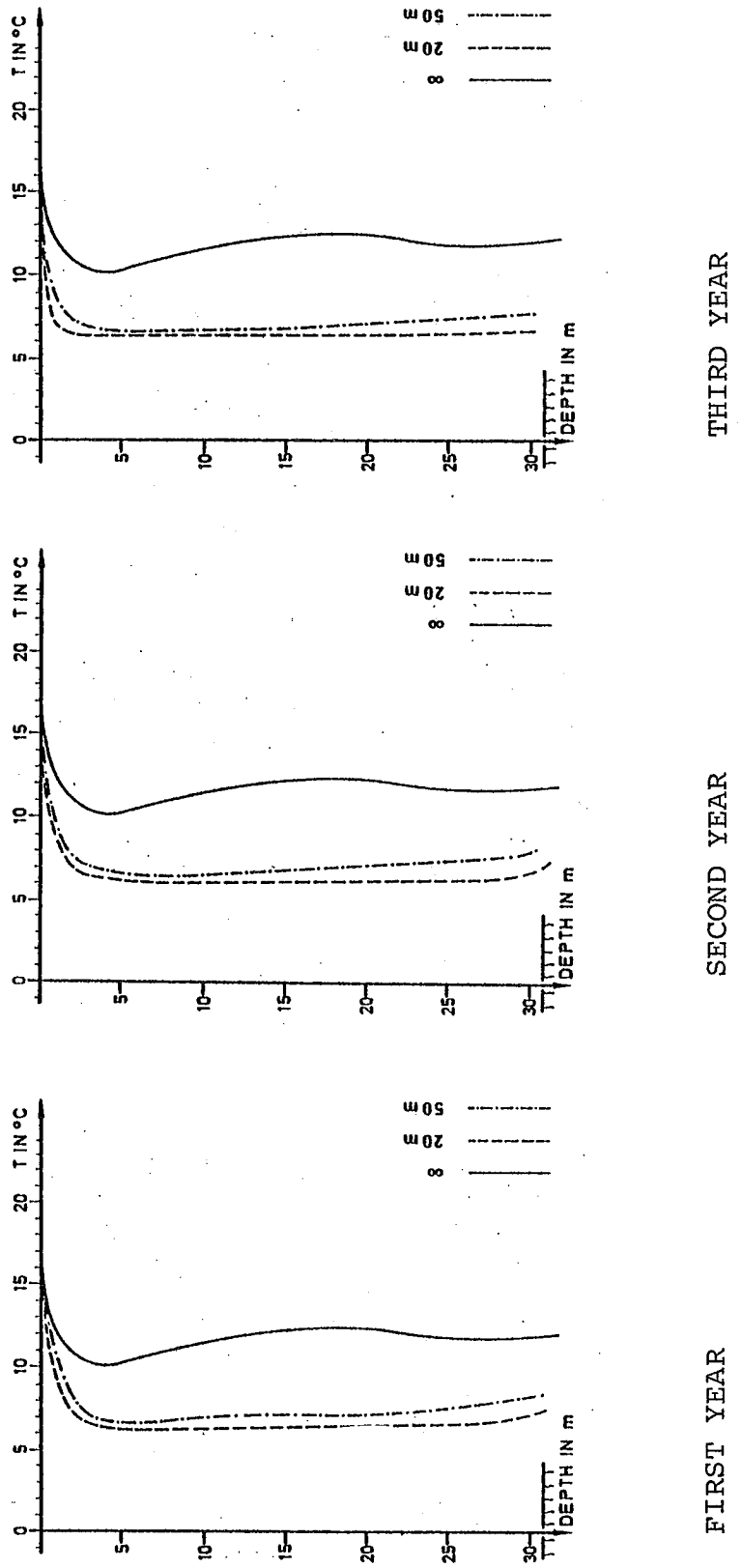

XBL 808-11182

Figure 25c. Temperature distribution in vertical cross-sections (May 15).

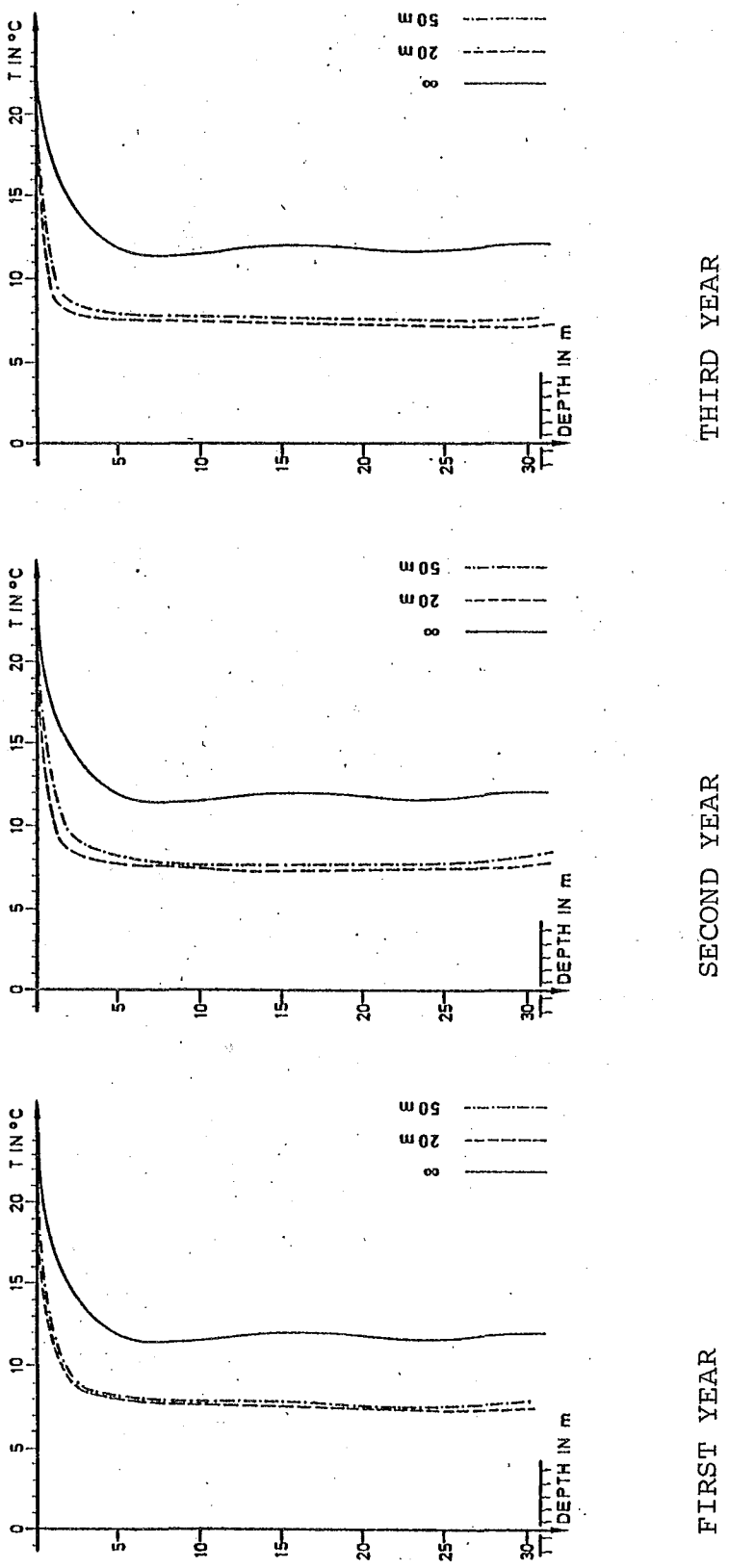

XBL 808-11183

Figure 25d. Temperature distribution in vertical cross-sections (July 15).

5.6 Cold and Warm Water Storage

5.6.1 Problem

Although the results, obtained for a two well storage system as illustrated in Figure 7, are satisfactory for the chosen example, the question arises as to whether the extended two-well storage system shown in Figure 8 can prove to be economically superior. In winter the water injected into the cold water well after use is cooled down by a secondary heat exchanger nearly to the temperature of the air. The reason for doing this with a secondary heat exchanger as opposed to the heat pump itself is because the performance coefficient of the heat pump drops dramatically with an increase in temperature difference.

In summer the water which is injected into the warm water well (after use for air conditioning) will be additionally heated nearly to air temperature by means of a heat exchanger.

Since 750 families can be supplied from this heat pump system, it is assumed that the wells can be installed at such distances as not to interfere with one another. For this case the thermal field around the wells can be calculated independently with the axisymmetrical three dimensional mesh used for the calculations of the previous examples. Otherwise, an arbitrary three dimensional mesh must be designed to encompass both wells.

5.6.2 Boundary Conditions

The description of the flux and heat transport boundary conditions at the lower, upper, and peripheral boundaries is identical to the previous example. Only the well is not described as an iteratively determined time-dependent Neumann condition and Dirichlet condition respectively. To allow easy comparison of the results with the heat fluxes and stored or extracted energies of the previous example, the calculations are carried out with the same fluxes that have been iteratively determined in the preceding calculations.

5.6.3 Results

As in the previous example three extraction/injection cycles are calculated. The overall calculation period is three years, starting in mid October with the first heating season.

Figure 26 shows the extraction/injection temperatures at the warm and cold water well. Since the calculation starts with the first heating season, no warm water has been recharged yet and the extraction is at the natural available ground water temperature. Later, the extraction temperatures at the cold and warm water well become a function of the extraction/injection history, heat losses, etc.

Using the fluxes calculated in the previous example (Figure 21), reasonably higher heat or cooling capacity injections and extractions are calculated as plotted in Figure 27.

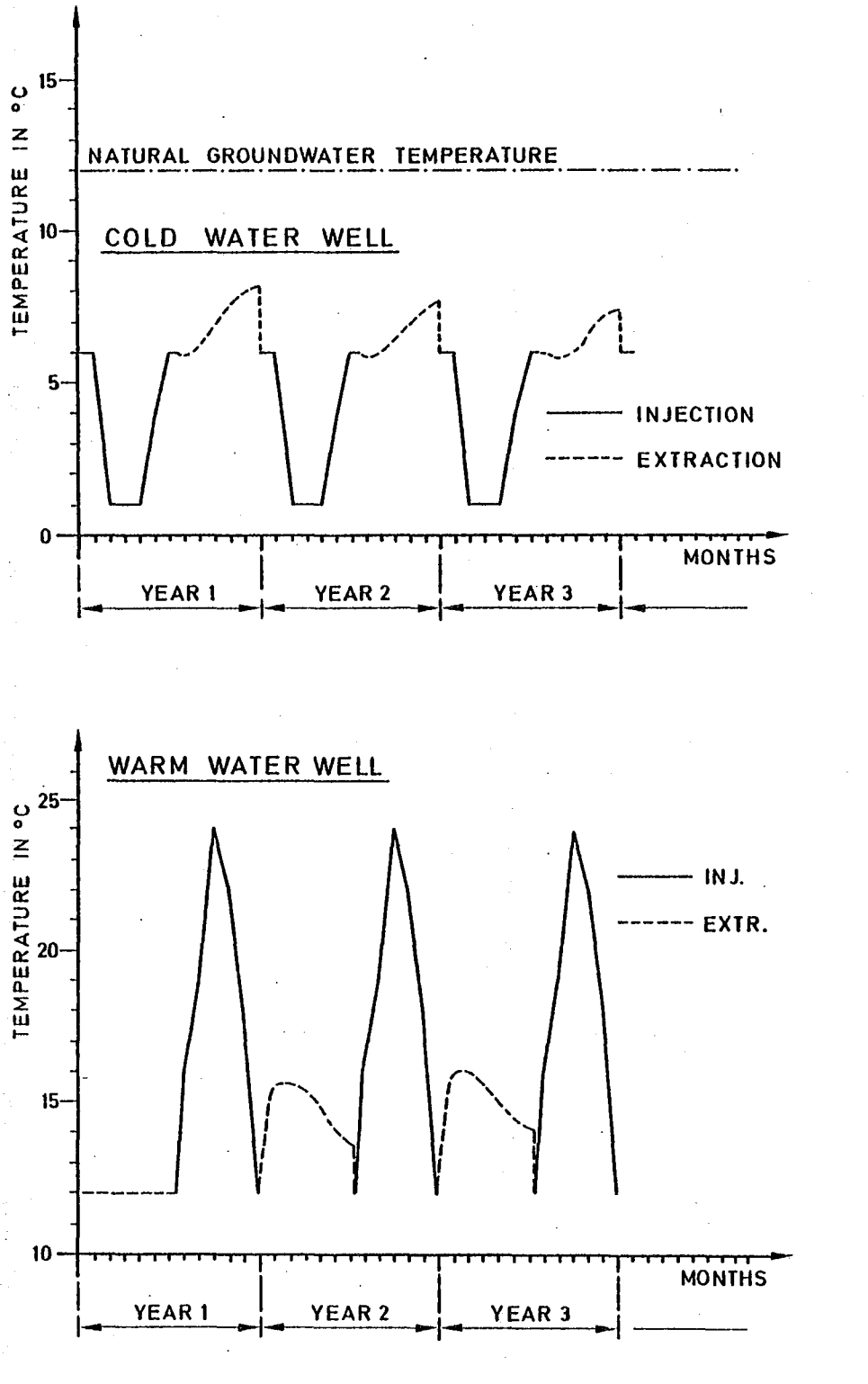

XBL 808-11170

Figure 26. Extraction and injection temperatures at the cold water well and warm water well.

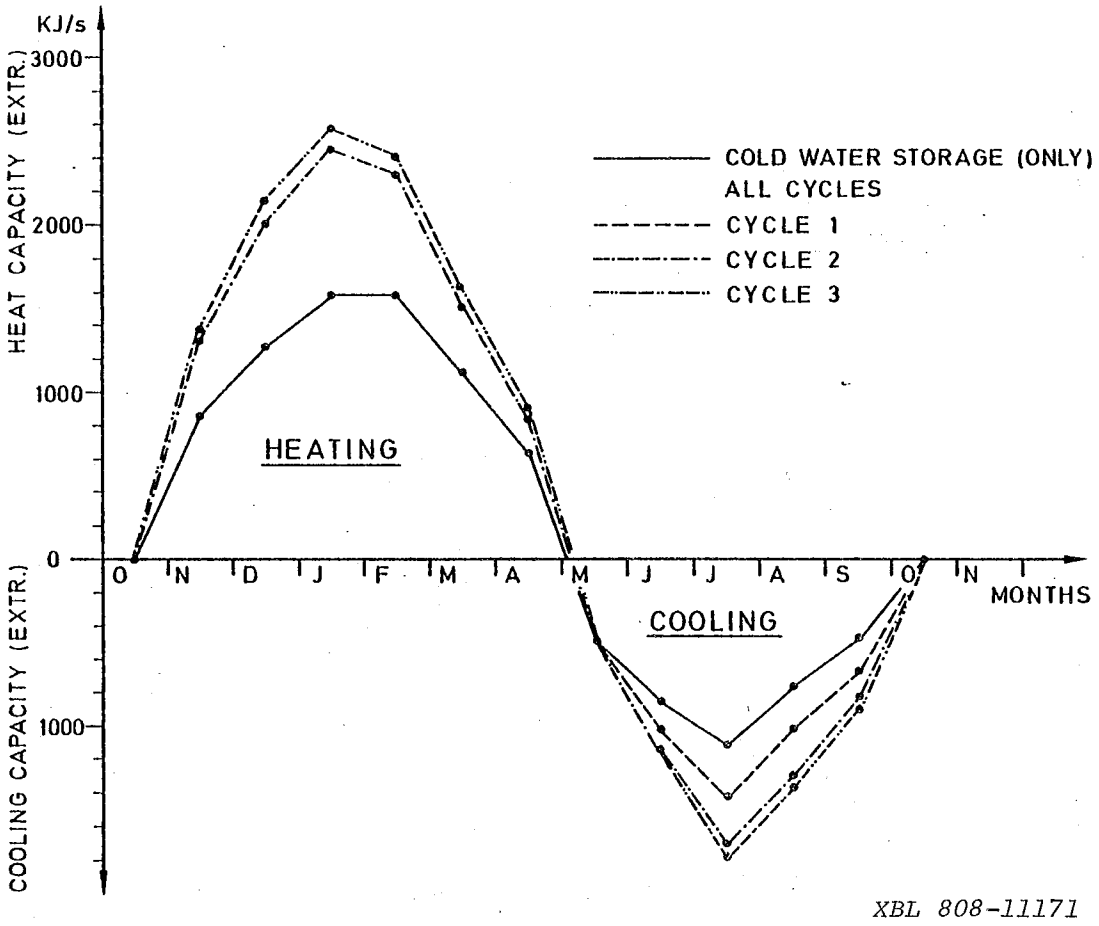

Figure 27. Heat fluxes for extraction periods.

In Figure 28 the cumulative curve of the additionally injected and extracted cooling capacity referenced to the natural average aquifer temperature, is plotted against time. This graph and the extraction temperature curve (Figure 26) show that with the current fluxes the cold water well is not completely developed.

The difference between injected and extracted cooling capacity is already partially lost to the environment. However, at the end of the summer cooling, capacity is still

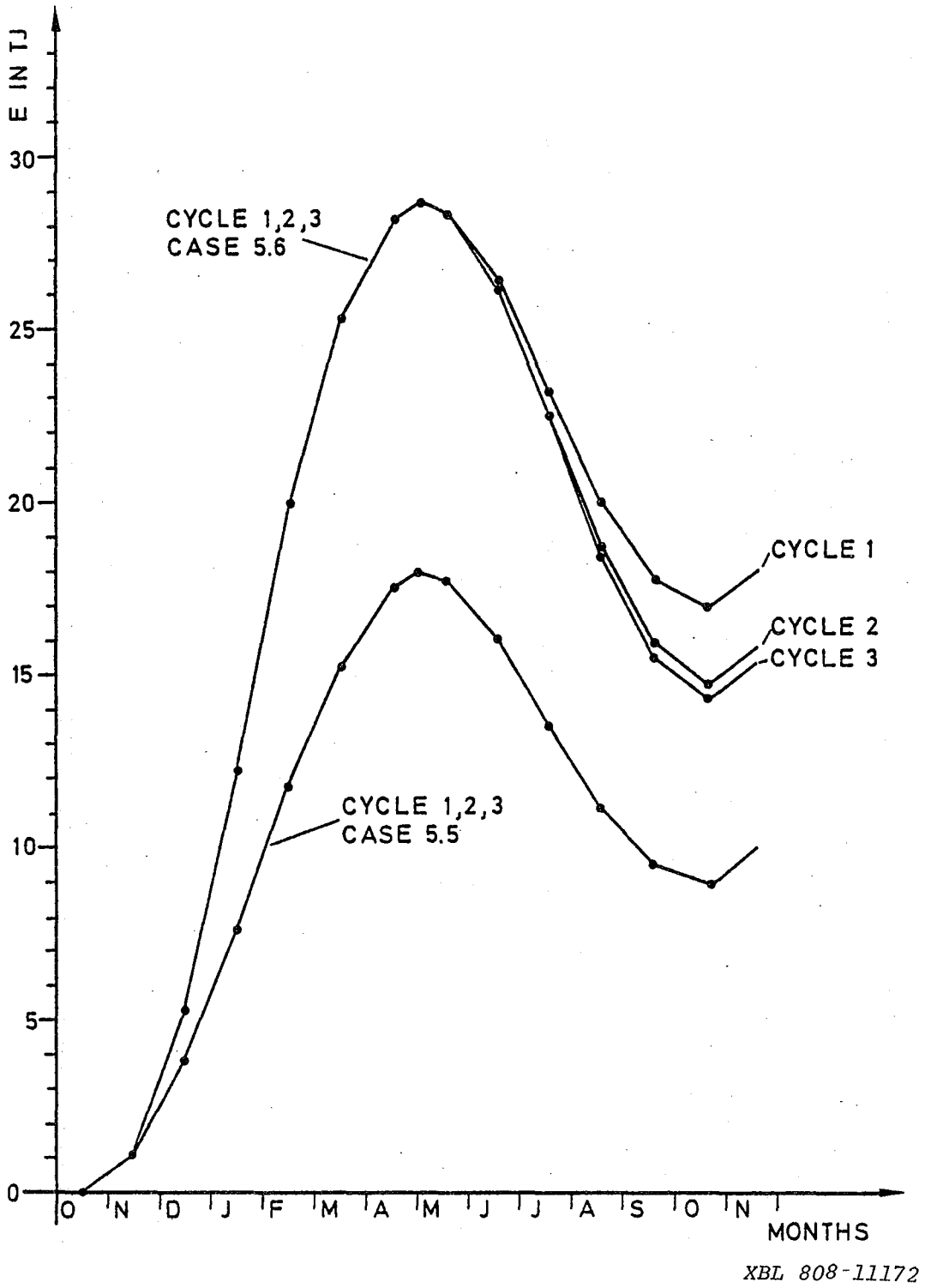

Figure 28. Cumulative curve of additionally injected and extracted cooling capacity at the cold water well.

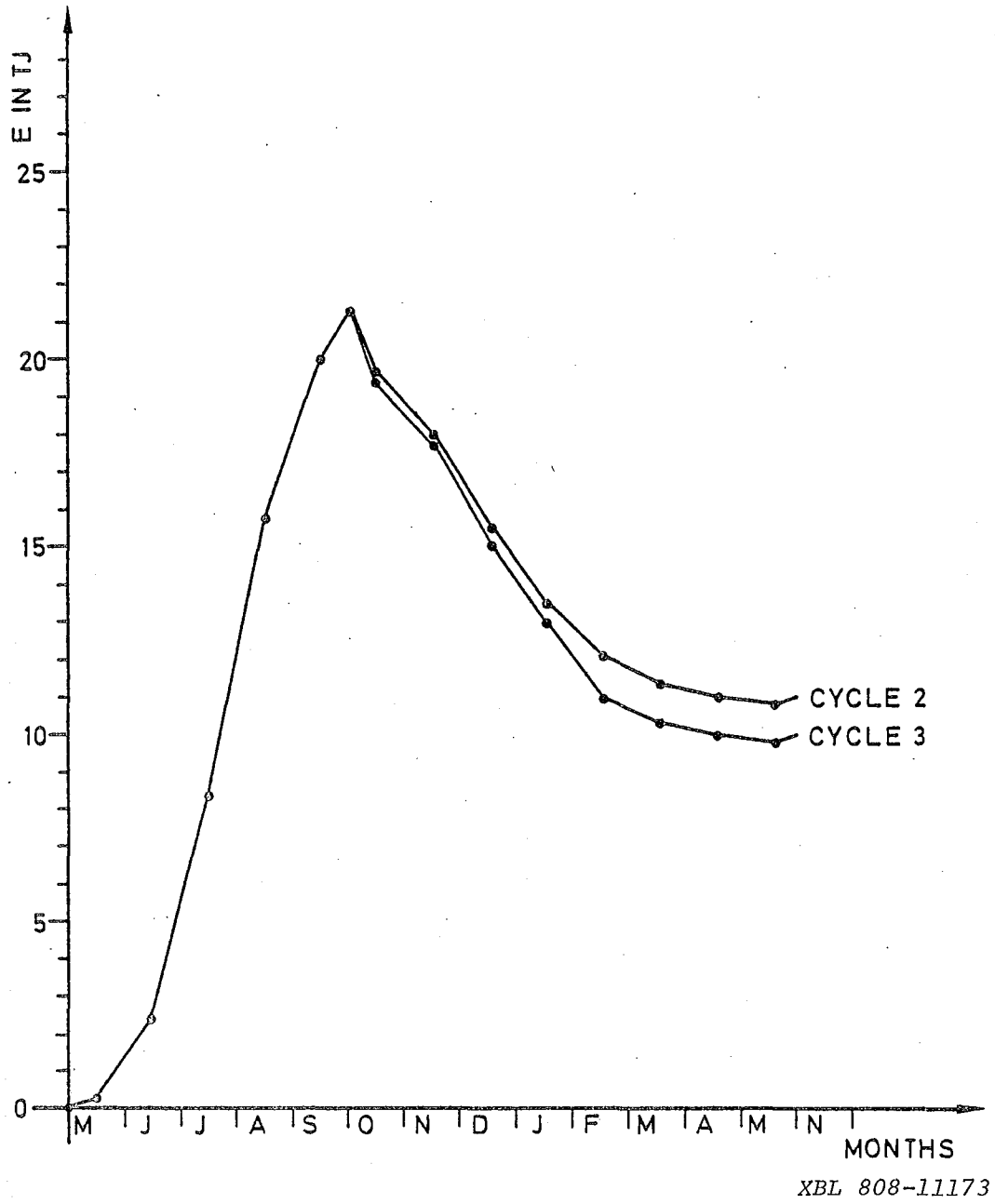

Figure 29. Cumulative curve of additionally injected and extracted energy at the warm water well.

available and could be extracted since the extraction temperature is far below the natural groundwater temperature of 12°C.

Figure 29 shows the cumulative curve of the additionally

injected and extracted energy referenced to the natural groundwater temperature, plotted against time.

In the previous example no additional energy was injected into the warm water well. Also, the first extraction cycle has to start with the natural groundwater temperature. It is obvious that the warm water well extraction also is not fully developed with the current fluxes. There is still part of the injected energy available at the end of the heating season, since the extraction temperature is higher than 12°C, the natural groundwater temperature. Nevertheless, one-third of the total extracted energy results from the additionally injected energy in summer as shown in Figure 30 and Table 5.

Due to the higher temperature gradients, the influences on the environment are stronger than in the previous case. The average vertical temperature of the saturated zone as a function of the radius and time is shown in Figure 31. Even in this example the thermal anomaly spreads very slowly after the second and third cycles.

This can also be seen in Figure 32, where the temperature in vertical cross sections is plotted against the depth below the surface. The changes of the temperature distribution are considerable and even in the unsaturated zone reach 5°C to 10°C. The temperature gradients, however, are relatively small, and buoyancy flow and the resultant tilting of the thermal front, as occurs in high temperature storage (7), is of minor importance. Other effects like hydrodynamical dispersion and changes in viscosity overshadow this phenomenon.

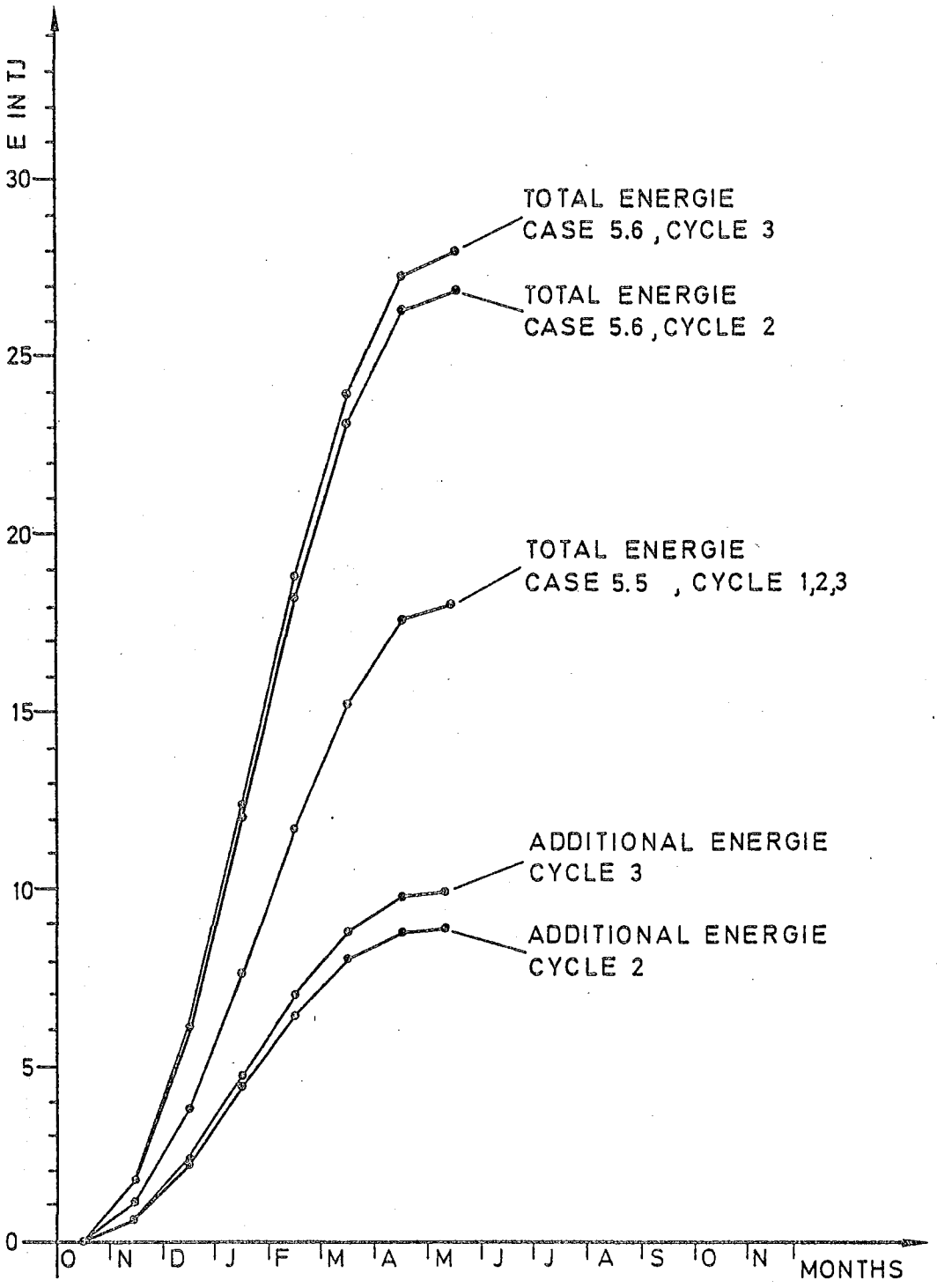

XBL 808-11174

Figure 30. Cumulative curves of total extracted energy at the warm water well.

EXAMPLE NUMBER	TOT. INJ. COOL. CAP.	TOT. EXTR. COOL. CAP.	ADD. EXTR. COOL. CAP.	TOT. INJ. ENERGY	TOT. EXTR. ENERGY	ADD. EXTR. ENERGY
---	TJ	TJ	TJ	TJ	TJ	TJ
5.5	18.03	9.06	----	----	18.03	----
CYCLE 1 5.6	28.63	11.61	2.55	----	18.03	----
CYCLE 2 5.6	28.63	13.78	4,72	21.29	26,89	8,86
CYCLE 3 5.6	28.63	14.20	5.14	21,29	27.93	9.90

Table 5. Total and additionally injected and extracted energy

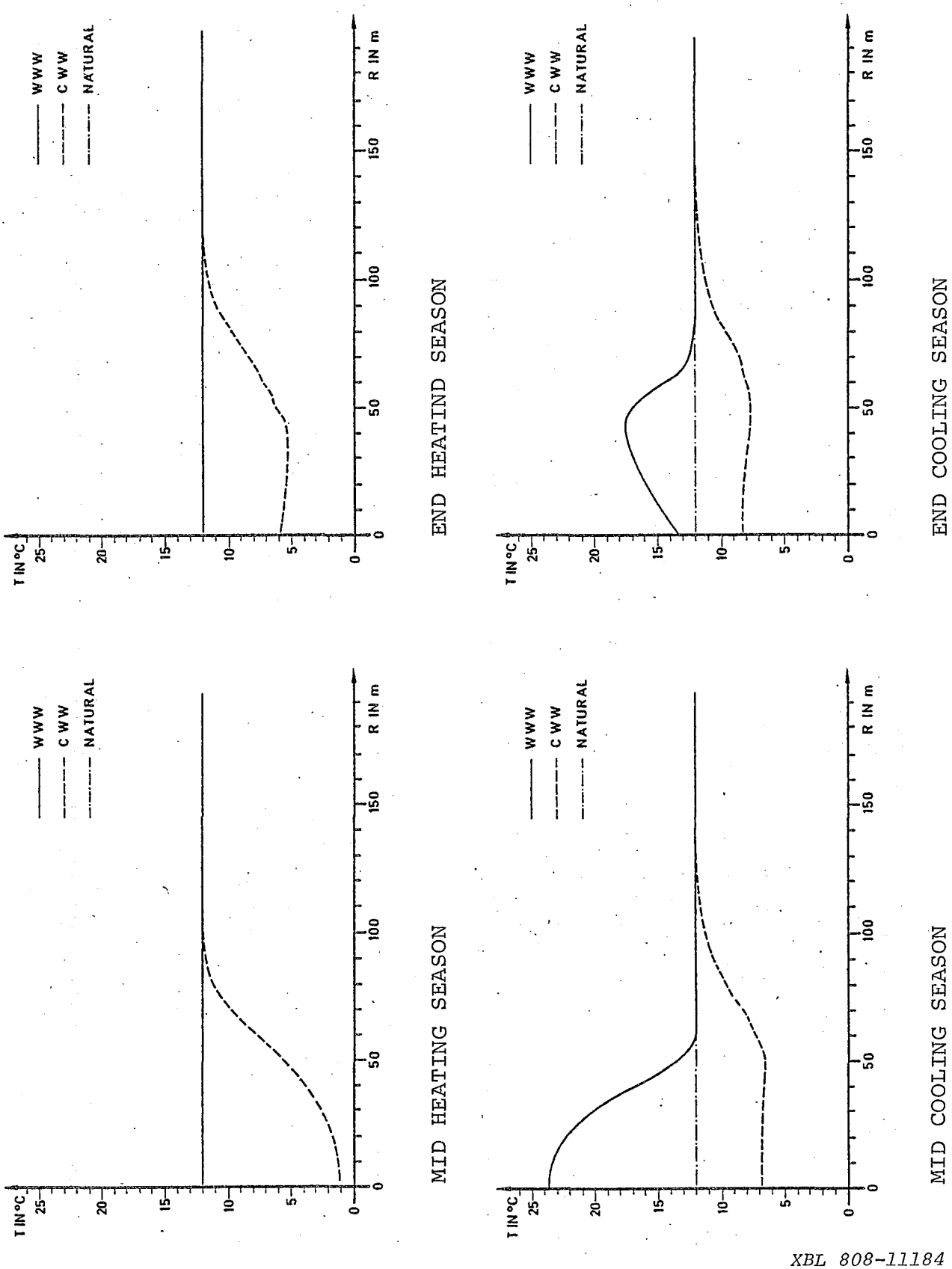

Figure 31a. Temperature as function of radius (first year).

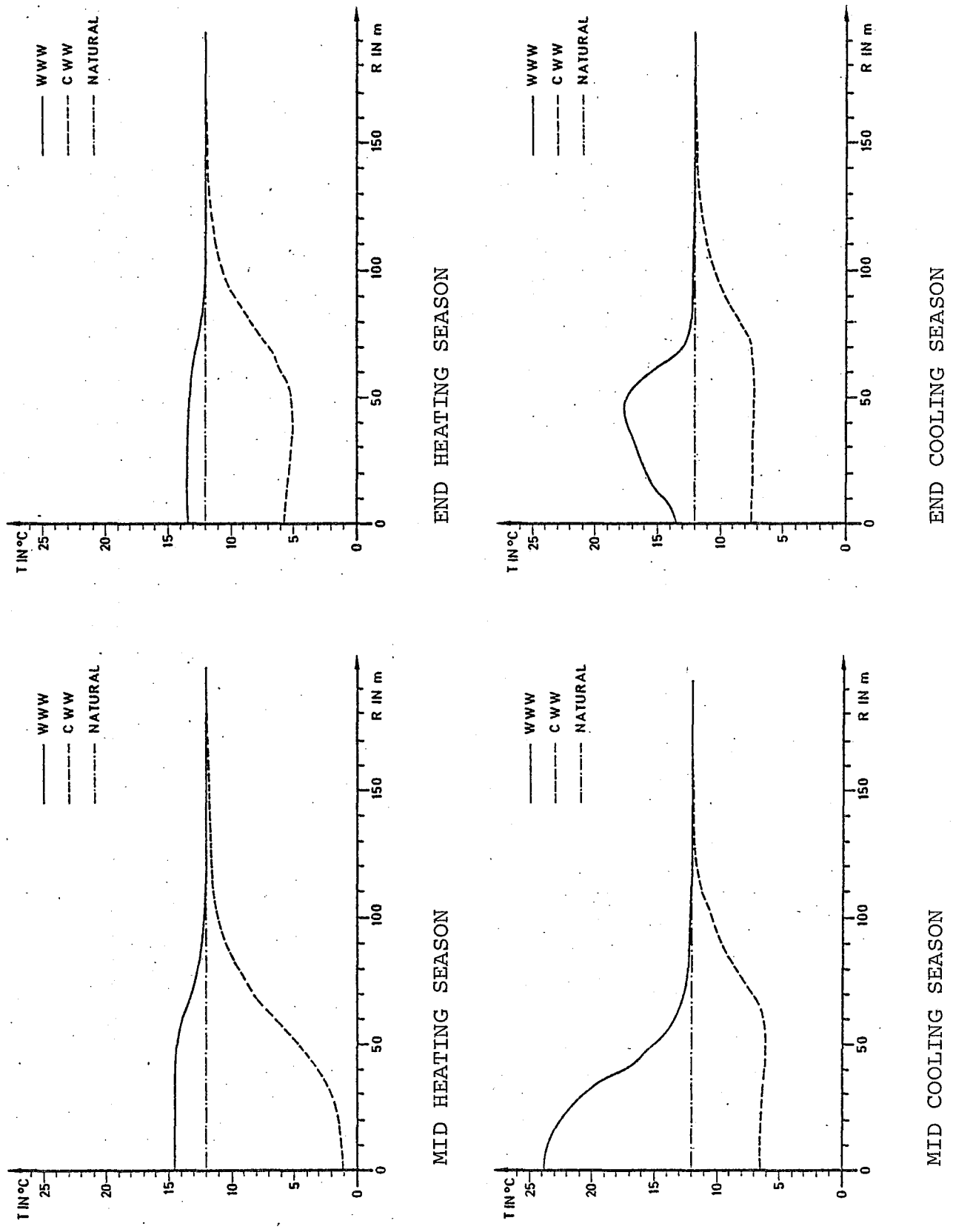

XBL 808-11185

Figure 31b. Temperature as function of radius (second year).

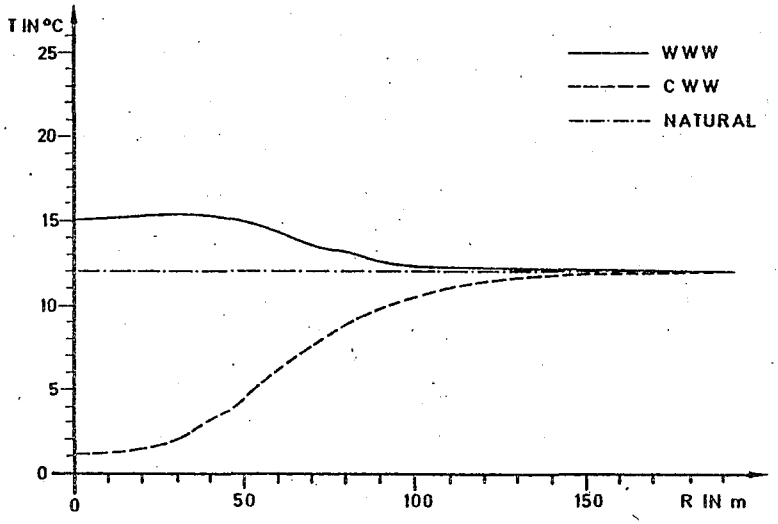

MID HEATING SEASON

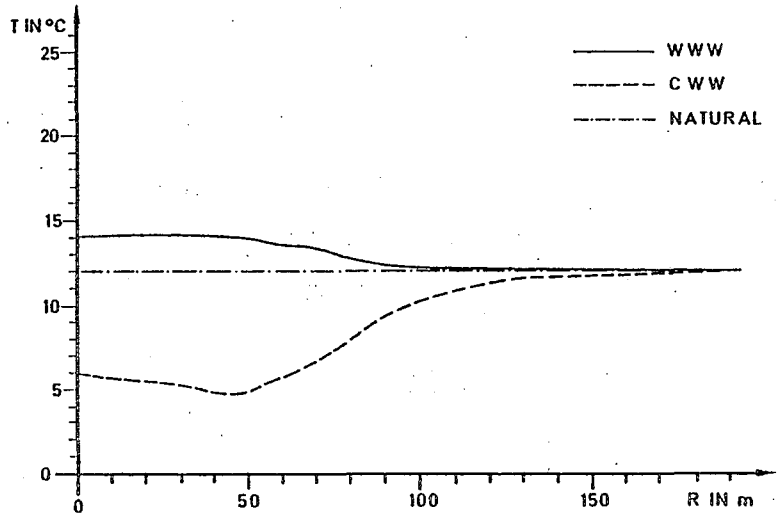

END HEATING SEASON

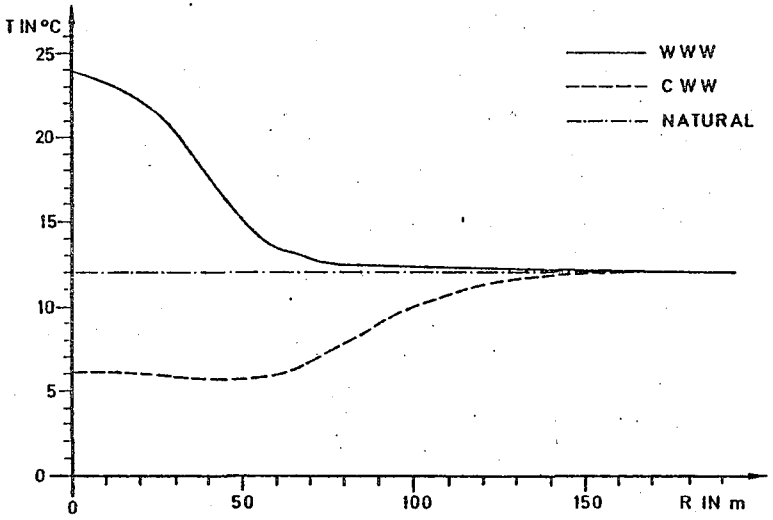

MID COOLING SEASON

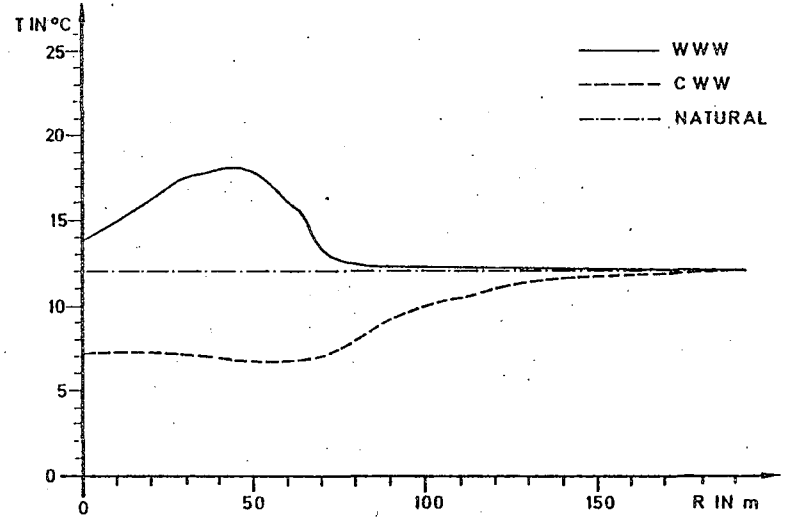

END COOLING SEASON

Figure 31c. Temperature as function of radius (third year).

XBL 808-11186

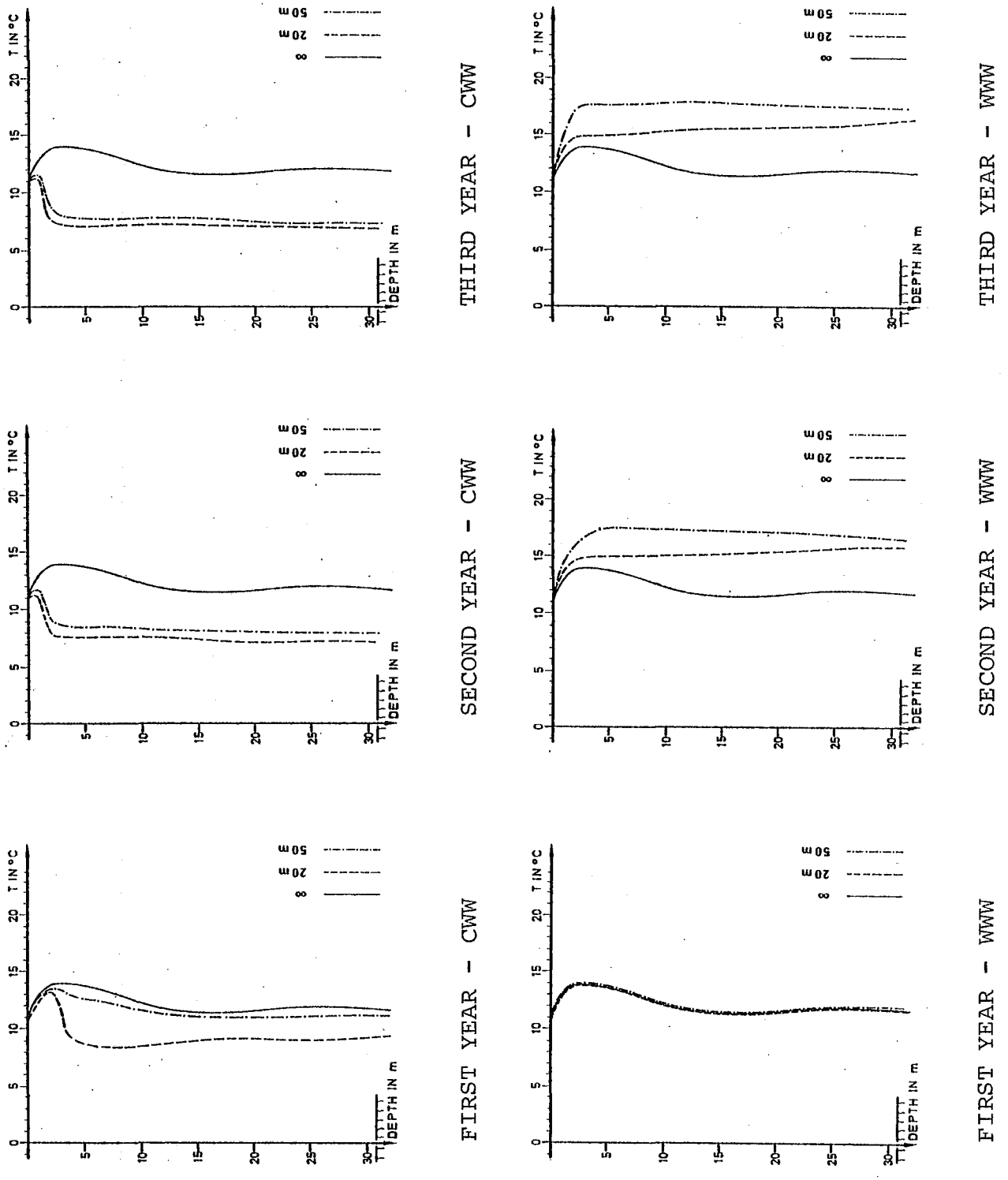

Figure 32a. Temperature distribution in vertical cross-sections (November 1).

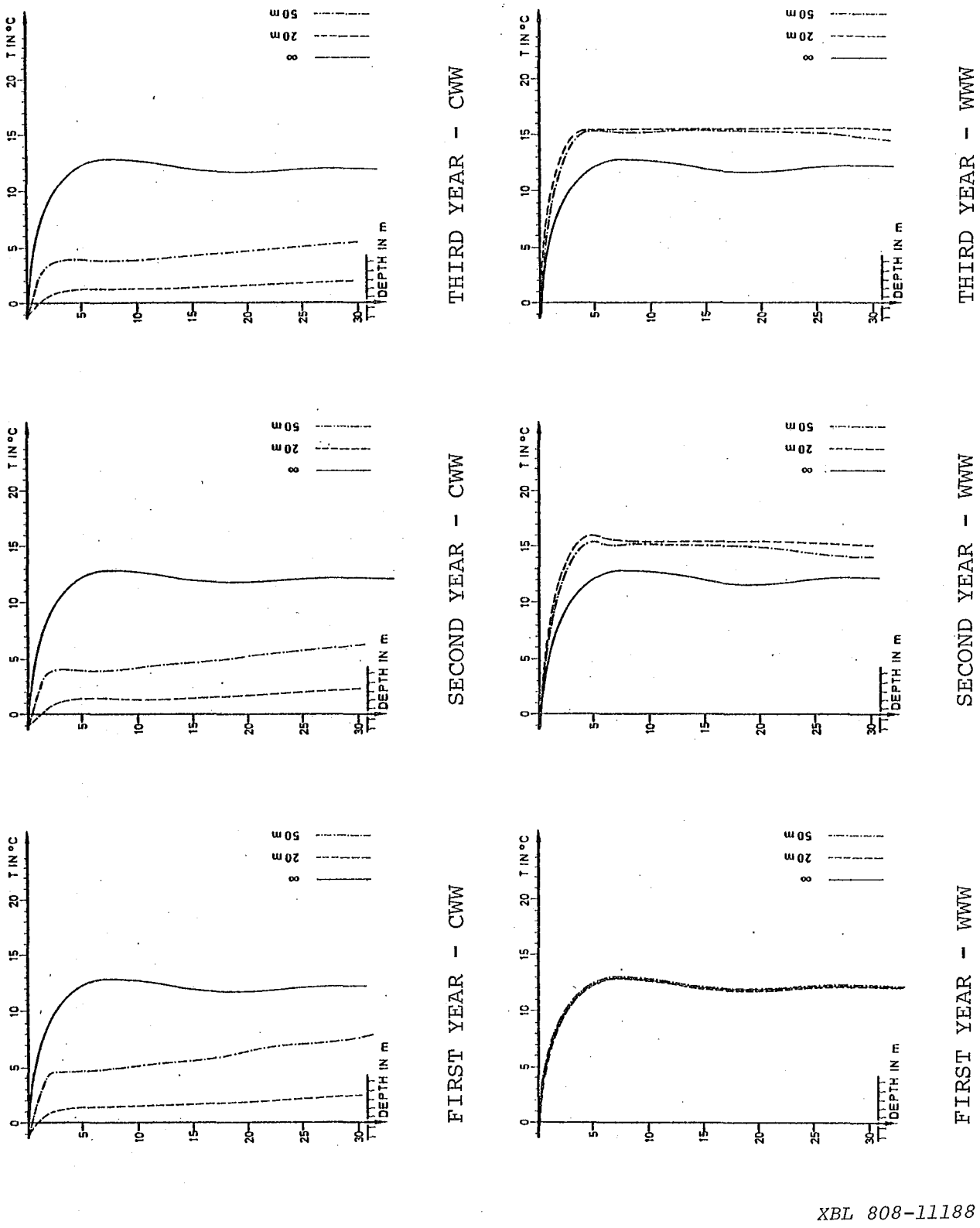

XBL 808-11188

Figure 32b. Temperature distribution in vertical cross-sections (February 1).

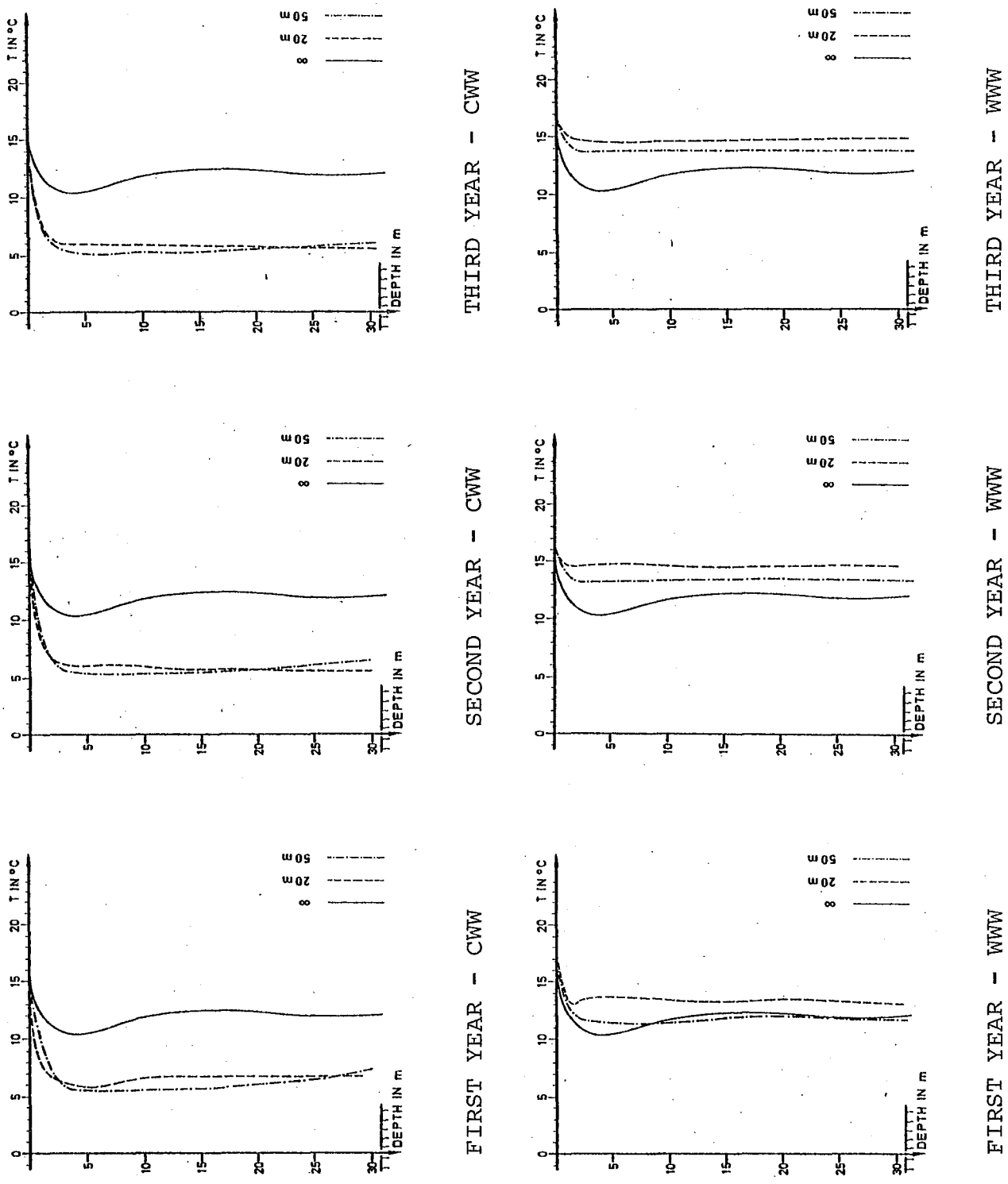

XBL 808-11189

Figure 32c. Temperature distribution in vertical cross-sections (May 15).

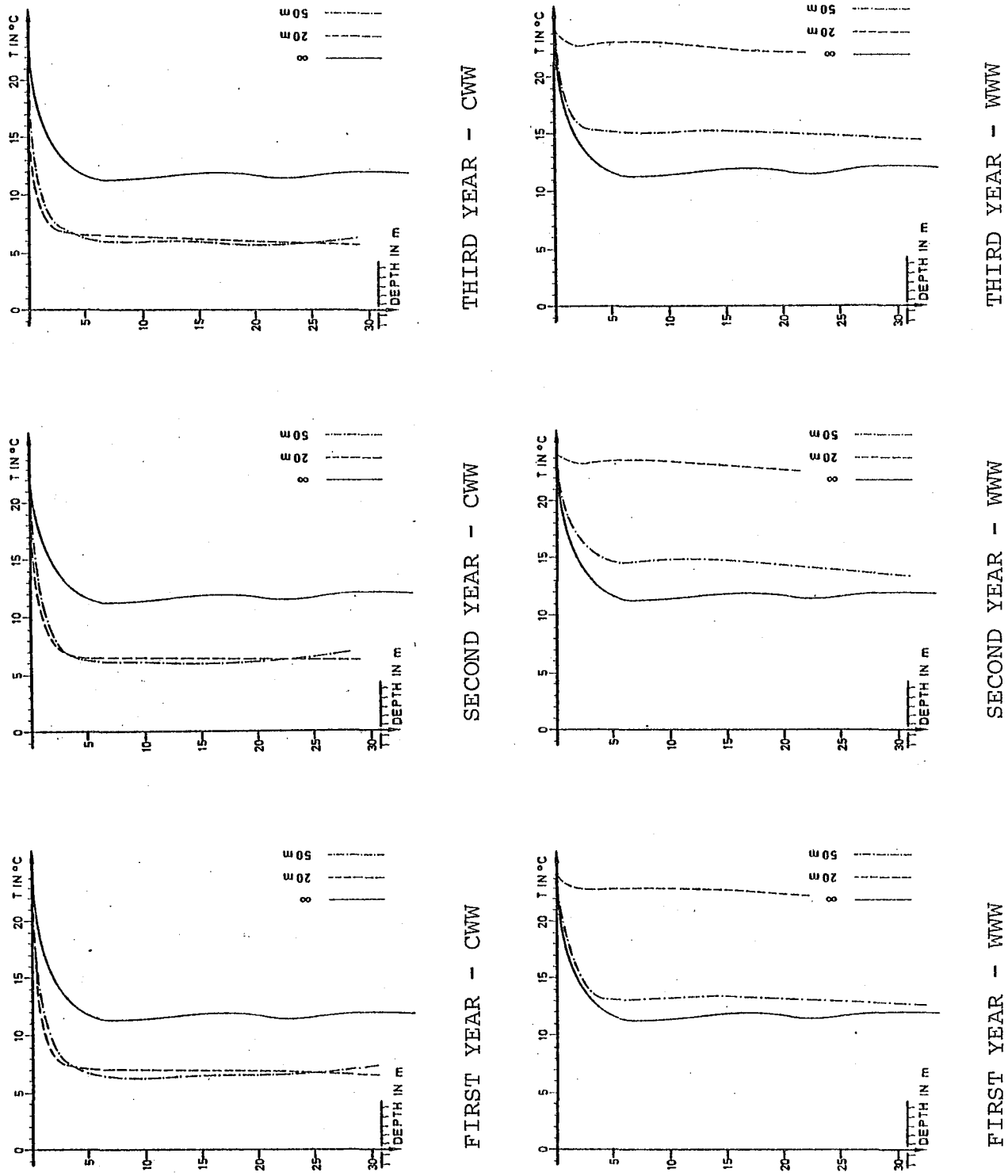

XBL 808-11190

Figure 32d. Temperature distribution in vertical cross-sections (July 15).

6. Conclusions

Two well storage systems with groundwater source heat pumps prove to be a realistic alternative form of energy for heating and/or air conditioning. The method is particularly applicable to northern climates, where heating is the principal load on the system. Additional storage of cooling capacity with a secondary heat exchanger in winter for air conditioning in summer, and storage of warm water in summer for heating purposes in winter may be economically advantageous.

The question of further improving the system raises several problems. An extended cooling capacity is limited by the available air temperatures and the freezing point of the injected water and can only be increased by larger injection volumes. Another possibility is the optimization of the cooling capacity input and output by adjusting the injection and extraction fluxes.

Improvements on the warm water side are not so difficult, since there is sufficient distance to the boiling point. Apart from an optimization as mentioned above, the temperature of the injected water simply could be raised. The restriction of the available air temperature could be overcome by replacing the secondary heat exchanger with a solar collector. Significant changes of the natural groundwater temperatures in the saturated and unsaturated zones are unavoidable and must be considered.

Numerical models are invaluable tools for the calculation of the changes of the flow and temperature fields in the aquifer. They enable the designing engineer to evaluate the influences of the planned system on the environment. Numerical methods are also powerful tools for the optimization of the recharge and discharge process. This optimization must take environmental requirements adequately into consideration.

The main uncertainties in the calculation are the heat transport in the unsaturated zone, interactions with meteorological data and exact determination of the boundary conditions. A more detailed study of these problems is left for further investigations.

LIST OF SYMBOLS

Indices, Coordinates

B	Bulk property
F	Fluid property
M	Solid matrix property
x, y, z	cartesian coordinates
i, j, k	Indices (for the three dimensional case i=1,2,3 j=1,2,3 k=1,2,3)
I, J	Node number

Scalars

a_I	Longitudinal dispersion factor
a_{II}	Transversal dispersion factor
A	Area
C	Heat capacity
h	Hydraulic reference head
p	Pressure head
Q	Sink/Source strength
S'	Storage coefficient
t	Time
T	Temperature
ε	Effective porosity
θ	Porosity
ρ	Actual density
ρ_o	Reference density
μ	Dynamic viscosity

Tensors, Vectors, Matrices

D_{ij}	Mechanical dispersion tensor
D_{ij}'	Effective dispersion tensor
g	Gravitational acceleration
k_{ij}	Specific permeability tensor
n	Normal vector
q_i	Average mass flux vector
v_i	Average fluid velocity vector
Λ_{ij}	Heat conductivity tensor
δ_{ij}	Kronecker delta symbol

Acknowledgements

The encouragement and interest of Paul Witherspoon are greatly appreciated. The assistance of V. Guvanasen in modifying his program for the special purpose of this project is gratefully acknowledged. Conversations with C. F. Tsang and the whole Geothermal Group of Lawrence Berkeley Laboratory formed part of the inspiration for this study.

This work was supported by the Wilhelm A. Vogt Foundation of the Rheinisch-Westfaelische Technische Hochschule, Aachen, Federal Republic of Germany.

The hospitality of the Earth Sciences Division of Lawrence Berkeley Laboratory and computational support from the U. S. Department of Energy (under contract W-7405-ENG-48) are gratefully acknowledged.

REFERENCES

1. Avdonin, N.A., Some formulas for calculating the temperature field of a stratum subjected to thermal injection. Neft'i Gaz, 3,37-4, 1964.

2. Balke, K.D., Die Abkuehlung des Untergrundes beim Betrieb von Grundwasser Waermepumpen. Elektrowaerme International 7, 9, 243-249, 1979.

3. Bear, J., Some experiments in dispersion. Journ. Geophys. Res. 66, 1961.

4. Electric Power Research Institut, An investigation of methods to improve heat pump performance and reliability in northern climate, EPRI-EM-319, Project 544-1, Final Report, 1977.

5. Gringarten, A.C., and Sauty, J.P., A theoretical study of heat extraction from aquifers with uniform regional flow. Journ. Geophys. Res. 80, 1975.

6. Guvanasen, V., Galerkin Finite Element Approach for heat and mass transport in deformable fractured rock masses. Seminar held at Lawrence Berkeley Laboratory, Earth Sciences Division, unpublished, 1980.

7. Hellstrom, G., Tsang, C.F., and Claesson, J., Heat storage in aquifers. Buoyancy flow and thermal stratification problems. Lund Institut of Technology, Department of Mathematical Physics, 1979.

8. Huyakorn, P., and Taylor, C., Finite element models for coupled groundwater flow and convective dispersion. Finite Elements in Water Resources, Proceedings of the First International Conference on Finite Elements in Water Resources, Princeton, U.S.A., 1976.

9. Luetkestratkoetter, H., Numerische Behandlung von Waermeausbreitungsvorgaengen in durchstroemten poroesen Medien nach der Methode der Finiten Elemente. Mitteilungen des Instituts fuer Wasserbau und Wasserwirtschaft, Rheinisch-Westfaelische Technische Hochschule Aachen, Heft 20, 1977.

10. Ogata, A., and Banks, R.B., A solution of the differential equation of longitudinal dispersion in porous media. U.S. Geological Survey, Professional Paper 411-a, 1961.

11. Rouve, G., Kerzel, C., and Pelka, W., Waerme aus Wasser und Boden-Gesichtspunkte zum Einsatz von Waermepumpen. Submitted to Wasser und Boden.

12. Segol, G., Pinder, G.F., and Gray, W.G., A Galerkin Finite Element technique for calculating the transient position of the saltwater front. Water Res. Res. 11, 1975.

13. Smith, I.M., Faraday, R.V., and O'Connor, B.A., Raleigh-Ritz and Galerkin Finite Elements for diffusion convection problems. Water Res. Res. 9, 1973.

This report was done with support from the United States Energy Research and Development Administration. Any conclusions or opinions expressed in this report represent solely those of the author(s) and not necessarily those of The Regents of the University of California, the Lawrence Berkeley Laboratory or the United States Energy Research and Development Administration.